

Article

Experimental Study on the Seismic Performance of Seismic Bracing in Important Buildings

Rongheng Liu ^{1,2}, Tao Jiang ^{1,2,*}, Junwu Dai ^{1,2}, Yongqiang Yang ^{1,2} and Wen Bai ^{1,2}

¹ Key Laboratory of Earthquake Engineering and Engineering Vibration, Institute of Engineering Mechanics, China Earthquake Administration, Harbin 150080, China; 17862702723@163.com (R.L.); junwu@iem.ac.cn (J.D.); yangyongqiang@iem.ac.cn (Y.Y.); baiwen@iem.ac.cn (W.B.)

² Key Laboratory of Earthquake Disaster Mitigation, Ministry of Emergency Management, Harbin 150080, China

* Correspondence: m18686805613@163.com

Abstract: Important buildings, such as hospitals and nuclear power facilities, must have basically intact pipe systems to function effectively after an earthquake. To study the seismic fragility and failure mechanisms of different typical seismic bracing system types, this paper conducts a comprehensive series of 34 monotonic and cyclic loading tests on four distinct configurations of seismic bracing. The bearing capacity performance and ductility of the components are evaluated thoroughly by using the area (energy) corresponding to the yield displacement, peak force corresponding displacement, and ultimate displacement of the force–displacement curve in the cyclic loading test. Ultimately, the results comprehensively assess the performance of various test specimens, offering suggestions to address the identified issues.

Keywords: seismic fragility; seismic bracing; cyclic loading test; engineering demand parameter; pipeline system



Citation: Liu, R.; Jiang, T.; Dai, J.; Yang, Y.; Bai, W. Experimental Study on the Seismic Performance of Seismic Bracing in Important Buildings. *Sustainability* **2023**, *15*, 9523. <https://doi.org/10.3390/su15129523>

Academic Editor: Constantin Chalioris

Received: 15 May 2023

Revised: 31 May 2023

Accepted: 7 June 2023

Published: 14 June 2023



Copyright: © 2023 by the authors. Licensee MDPI, Basel, Switzerland. This article is an open access article distributed under the terms and conditions of the Creative Commons Attribution (CC BY) license (<https://creativecommons.org/licenses/by/4.0/>).

1. Introduction

In the past several decades, seismic research on structural components has significantly advanced [1–4]; however, there has been limited attention paid to seismic research on nonstructural components (NSCs) that are more vulnerable to damage. In hospitals and other important structures, the pipeline system is an essential nonstructural component for maintaining fire protection and other operations, and these systems can sustain increasingly severe damage in consecutive earthquakes. Due to the growing proportion of economic investment in nonstructural systems in buildings, especially in significant buildings, the seismic resilience of NSCs has become a fundamental concern for functional and economic losses in such buildings. According to FEMA E-74 Reducing the Risks of Nonstructural Earthquake Damage [5], structural components of commercial buildings generally account for 15–25% of construction expenditures, while NSCs (mechanical, electrical, and plumbing) account for 75–85% of the remaining expenses (Figure 1). After the 1971 San Fernando earthquake, a survey of 25 damaged commercial buildings revealed the following breakdown of economic losses: structural damage, 3%; electrical and mechanical damage, 7%; external finishes, 34%; and interiors, 56%. A similar survey of 50 damaged high-rise buildings found that while no significant structural damage occurred to the main structure, 43 of the buildings had damaged gypsum board partitions, 18 had damaged elevators, 15 had broken windows, and 8 had damaged air conditioning systems [6]. Consequently, during earthquakes, NSCs are often more sensitive to damage than structural components.

If the building's main structure stays substantially intact during an earthquake, the building's capacity to continue normal operations frequently depends on the integrity of the piping system, ceiling system, partition walls, and other nonstructural components (NSCs). Especially in hospitals, airports, and other important buildings, the ability of the

building to maintain normal operations is a prerequisite for efficient post-earthquake rescue and restoration.

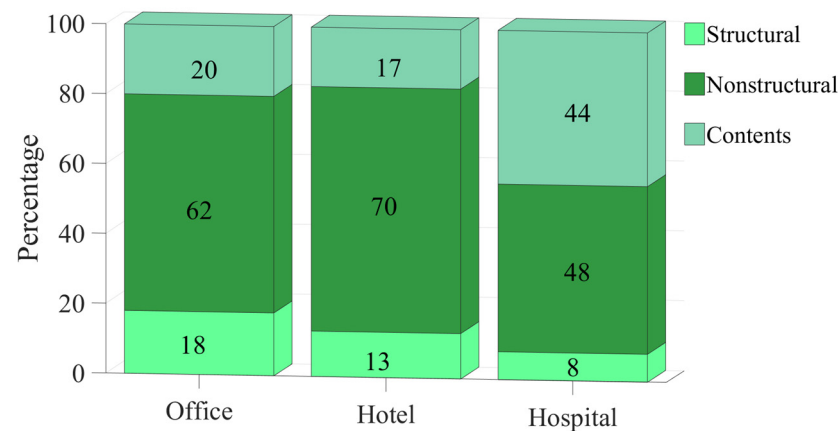


Figure 1. Composition of economic losses due to earthquakes [5].

The Sichuan province county health center lost basic function after the 2013 Lushan Ms 7.0 earthquake due to substantial damage to the piping and ceiling systems [7]. Even if the primary structure can be used immediately after an earthquake, damage to NSCs, particularly the piping system, can reduce or eliminate the building's functionality. The damage to piping systems under earthquake action can be typically divided into three categories: (1) failure of supports such as suspension, lateral, or longitudinal in piping systems; (2) failure of piping systems due to collision with the main structure or other NSCs that may cause large displacements in earthquakes; and (3) failure of piping systems due to uncoordinated deformation that may result from setting unreasonable restraints. Although there are existing relevant codes for the seismic design of pipe systems, past earthquakes demonstrate that the seismic performance of piping systems must be improved.

Pipeline systems generally consist of pipeline structures, fluids, valves, other accessories, and system support systems. Chen S, Xu, and Ye [8–10] studied the performance of underground pipeline systems. Numerous researchers have studied flow transmission pipes [11,12], but less attention has been paid to water supply systems, which are functional under normal conditions but easily damaged by earthquakes.

Tian et al. [13] conducted dynamic tests on three groups of fire-extinguishing sprinkler piping systems using different supports, and their results proved that seismic bracing can considerably improve the seismic resistance of piping systems. Tian et al. [14] conducted monotonic and reciprocal loading experiments on 48 tee joints of varied diameters, materials, and connections to assess the rotational capability of such specimens following initial leakage. Hoehler et al. [15] conducted shaking table tests on pipe systems installed in seven-story reinforced concrete structures to determine their damage modes at varying seismic intensities and analyzed the test data to determine the accuracy of the acceleration calculation method for NSCs in the ASCE 7-05 code [16]. Daniele et al. [17] conducted a series of quasi-static tests on various types of seismic bracing systems using different types of portal seismic bracing systems (braces are screws and channels) with the actuator loaded in the direction of the tube and perpendicular to the tube; their results concluded that the effective ductility factor in FEMA P-795 [18] is more conservative as an engineering demand parameter. Numerous Chinese scholars have also conducted research on seismic pipe system topics. Shang Qingxue et al. [19] conducted multiple sets of quasi-static tests on three types of seismic supports, namely, the screw type, the steel cable type, and the beam clamp type, but the tests did not account for the influence of pipe clamps, pipes, etc., and only evaluated the seismic performance of the bracing. Wu Houli et al. [20] evaluated the performance of water supply pipes in full-scale masonry constructions by using shaking table tests.

Ensuring the basic functionality of the water supply pipeline system after an earthquake is a fundamental prerequisite for important buildings such as hospitals to achieve their basic functions. Currently, research on the seismic resilience of buildings has become increasingly in depth, and FEMA P 58 provides a large database of NSC fragility based on U.S. standards. However, seismic bracings, as a commonly used seismic restraint device for pipeline systems, have various structural forms, and there are certain differences in the seismic bracings used in important buildings in different countries [21]. Therefore, assessing the seismic resilience of pipeline systems in important buildings requires data on the fragility of seismic braces that comply with U.S. standards. Nevertheless, there is little research on seismic bracing, and no research has been conducted on the four types of seismic bracing systems used in this study. The expansion of the NSC fragility database still requires a large number of experiments. Meanwhile, determining appropriate engineering demand parameters remains a worthy exploration in relevant research. Daniele et al. [17] studied seismic bracings with small differences in two mechanical properties using the equivalent ductility coefficient as the engineering demand parameter. Whereas the equivalent ductility coefficient only considers the deformation capacity of the components, without including the load-bearing capacity, which is also an important measure. For a situation where a test specimen has low load-bearing capacity but strong deformation capacity, the reasonableness of using the equivalent ductility coefficient as the engineering demand parameter is questionable.

Currently, the research on the seismic performance of pipeline systems mainly relies on shaking table tests as the primary method. In addition, there exist significant differences in the construction of pipeline systems tested by different scholars. As a result, insufficient understanding still exists regarding the seismic damage mechanism of different pipeline systems, especially those that use new seismic bracings. Therefore, this study conducted quasi-static tests on four typical types of new seismic bracing systems with energy values (force–displacement envelope area) that simultaneously considered the bearing capacity and deformation capacity of seismic bracings as engineering demand parameters. Moreover, the fragility of each specimen was obtained based on the energy values, and the damage mechanisms of each specimen were analyzed through the experiment. Finally, improvement suggestions were proposed for the weaknesses of each type of specimen.

2. Test Specimens

Two different designs of single-tube seismic bracings, named S1 and S2, and two different configurations of portal seismic bracings, designated M1 and M2, were evaluated in this paper. Each type of seismic bracing could be divided into longitudinal direction (X-direction) and lateral direction (Y-direction) specimens for a total of eight test cases. Table 1 is a summary of the test specimens.

Table 1. Test cases summary.

Seismic Bracing		Monotonic	Quasi-Static
Single-tube seismic bracing	S1-X	1	3
	S1-Y	1	3
	S2-X	1	3
	S2-Y	1	3
Multi-tube seismic bracing	M1-X	1	3
	M1-Y	1	3
	M2-X	1	3
	M2-Y	1	3

2.1. Single Tube Seismic Bracing

2.1.1. S1 Test Specimen

This type of seismic bracing mainly consists of anchor bolts (which are substituted with bolts during the actual test), channel steel, seismic connectors, screws, screw fasteners,

torsional shear clip, pipe clamps, and hexagonal connection nuts. The effective installation height of the seismic bracing is 750 mm, and the screw is installed at nearly 45° to the diagonal brace, as detailed in Figure 2. To prevent the vertical screw from buckling prematurely, 650 mm of C-channel steel and two screw fasteners are installed on the vertical screw. Meanwhile, the lateral (longitudinal) supports are connected to the lower part of the screw by seismic connectors, and the upper part of the lateral (longitudinal) supports are connected to the top cut-bottom anchor bolts by upper seismic connectors. Furthermore, the top and lower seismic connectors are connected through C-channel steel. In addition, two torsional shear clips are installed in the diagonal support channel to prevent an excessive amount of relative movement between the upper and lower seismic connectors and the channel steel during an earthquake. Rubber matting encases the pipe clamps, which are then bolted to the water pipe on both sides of the pipe bundle. When all bolts have been tightened to the appropriate tension (40 N·m) according to the installation standards, the installation process is complete.

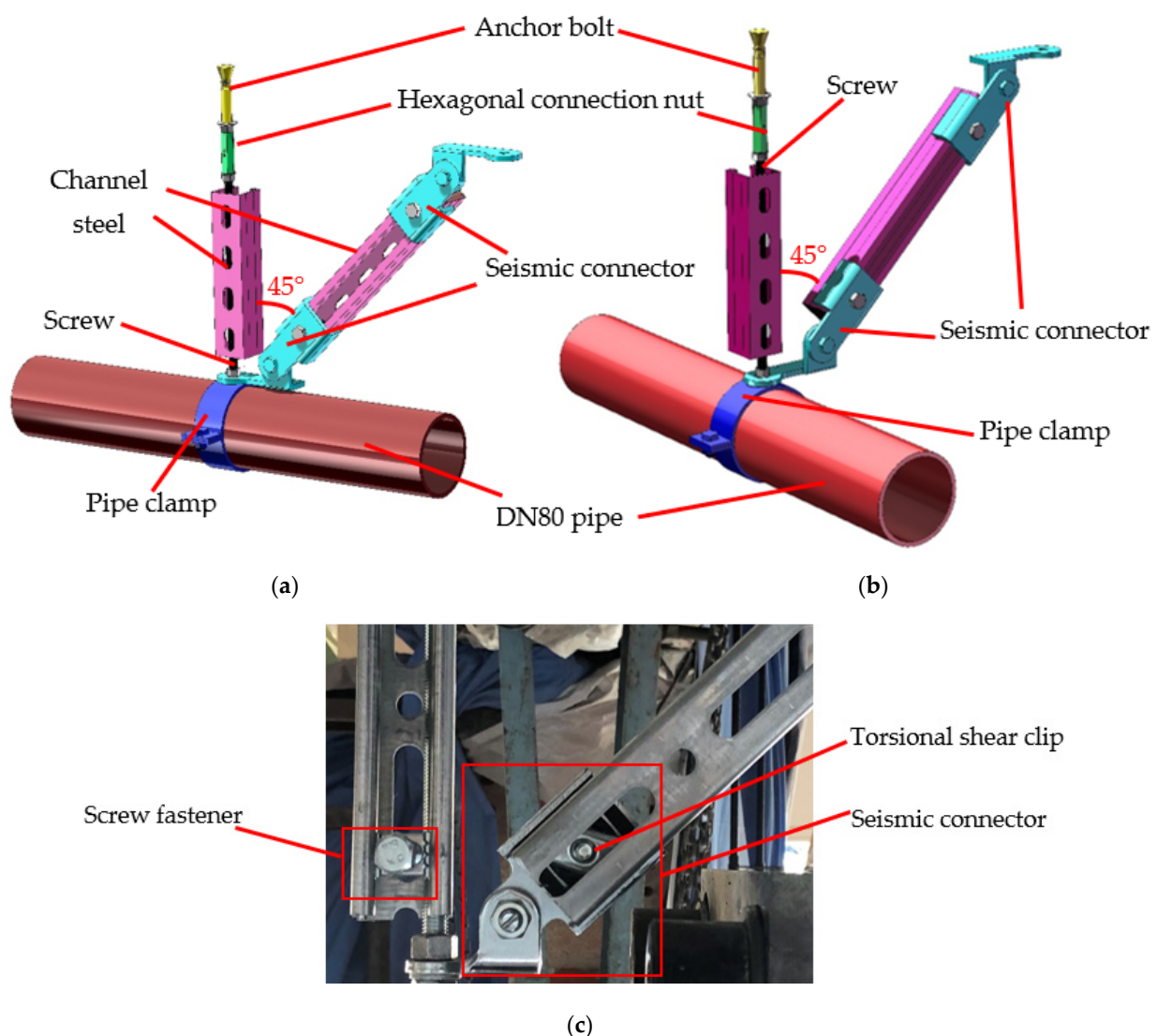


Figure 2. Test specimen of S1. (a) Test specimen of S1-X; (b) test specimen of S1-Y; and (c) detail of the bracing components.

2.1.2. S2 Test Specimen

The S2 seismic bracing consists of anchor bolts (replaced by bolts during the actual test), hot-dip galvanized U-channel steel, seismic connectors, screw fasteners, pipe clamps,

and hexagonal connecting nuts. The screw is set at an angle of around 45° to the diagonal bracing, giving the seismic bracing an effective installation height of 750 mm. To increase the initial stiffness of the vertical suspension member and prevent the vertical screw from buckling too early, 650 mm U-channel steel and 2 screw fasteners are installed on the vertical screw and connected to the M10 screw by a hexagonal connection nut on top of the top anchor bolt.

The lateral (longitudinal) support is connected to the lower end of the screw through the seismic connector, and the upper part of the lateral (longitudinal) support is connected to the top cut-bottom anchor via the upper seismic connection. To prevent them from producing excessive relative displacement when subjected to seismic action, the upper and lower seismic connections are bolted to the channel between the upper and lower seismic connections. The pipe clamps, like the S1 specimen, are fastened to the pipe on both sides of the bundle using bolts. Every bolt is torqued and tightened in accordance with the installation requirements (the torsion is not explicitly stated). The specimen's installation diagram is shown in Figure 3.

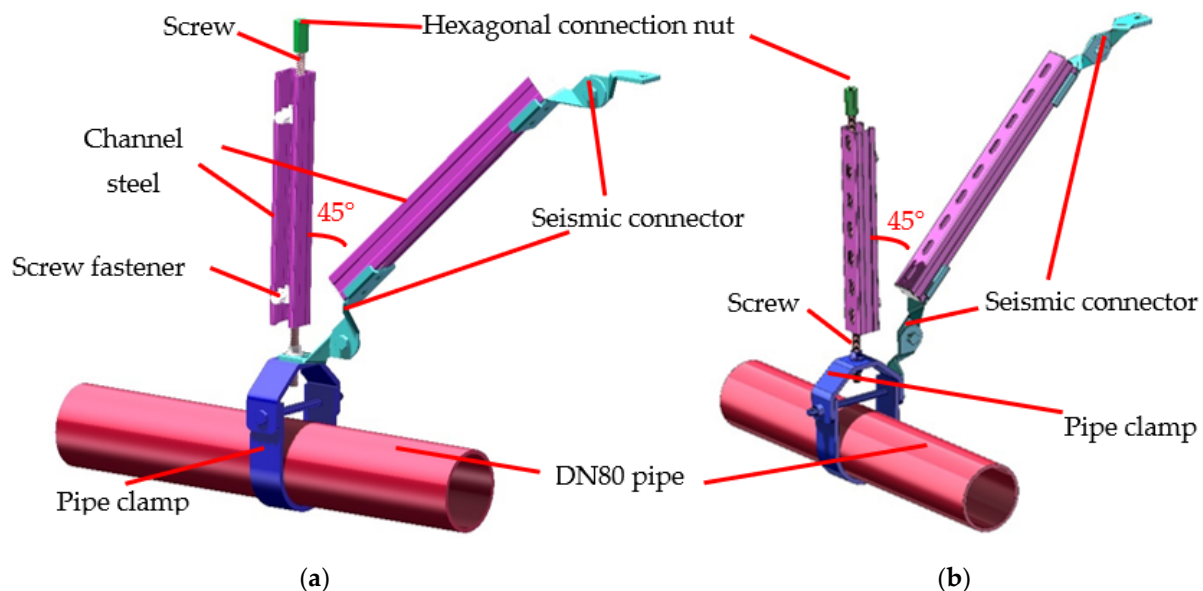


Figure 3. Test specimen of S2. (a) Test specimen of S2-X; (b) test specimen of S2-Y.

2.2. Multi-Tube Seismic Bracing

2.2.1. M1 Test Specimen

The M1 seismic bracing mainly consists of anchor bolts, steel base, torsional shear clip, seismic connection kit, seismic connectors, and pipe clamps. Through the anchor bolts, the steel base is joined to the top of the structure. In contrast with the S1 specimen, the vertical suspension is directly attached to the steel base through torsional shear clips. The seismic bracing of the M1 type consists of 3 DN80 pipe clamps positioned above the horizontal channel steel and 2 vertical suspension supports connected to the horizontal channel steel by a seismic connection kit. The M1 seismic bracing's longitudinal and transverse support is nearly identical to that of the S1 single tube type support. The effective installation height of M1 is 750 mm and the installation is finished when all the nuts are tightened and the torsion reaches the installation criterion (40 N.m). The installation diagram for the test item is shown in Figure 4.

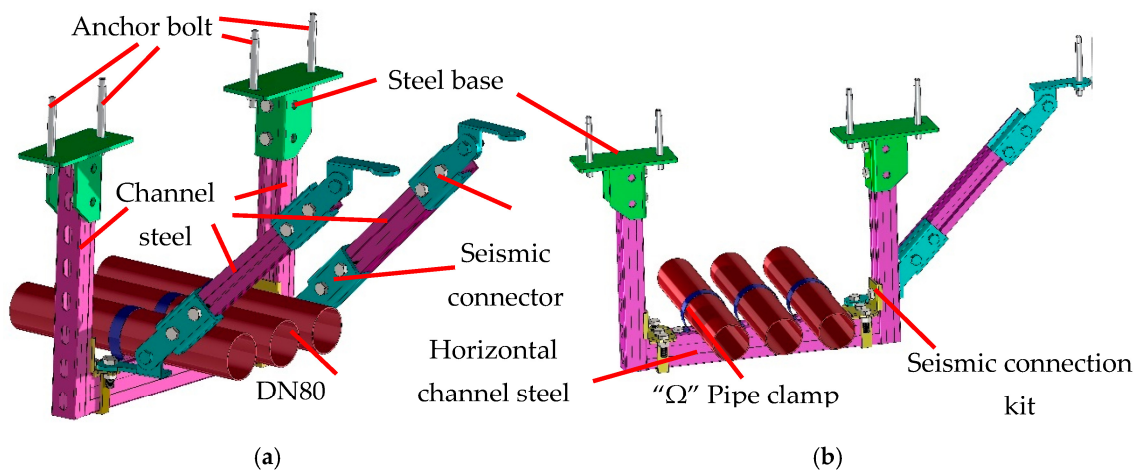


Figure 4. Test specimen of M1. (a) Test specimen of M1-X; (b) test specimen of M1-Y.

2.2.2. M2 Test Specimen

The M2 seismic bracing is composed of anchor bolts, hot-dip galvanized U-channel steel, seismic connectors, wire rod compression bolts, hexagonal connection nuts, and DN80 pipe clamps. The two vertical suspension supports are connected to the horizontal channel steel attached to the lower wire rod, and the vertical suspension support is connected to the top anchor bolt through the hexagonal connection nut. The lower portion of the horizontal channel steel attached to the wire rod is held in place by the channel steel cover plate. The longitudinal diagonal bracing is the same as the horizontal bracing. Additionally, galvanized channel steel is fitted with seismic connectors on both the higher and lower ends. At the location of the upper channel steel cover in the vertical suspension bracing, the upper connection is attached to the top anchor bolt, and the lower connection is connected to the horizontal channel steel. The installation angle for the horizontal and longitudinal bracing is close to 45 degrees, and the effective installation height is 750 mm. The installation diagram for the test item is shown in Figure 5.

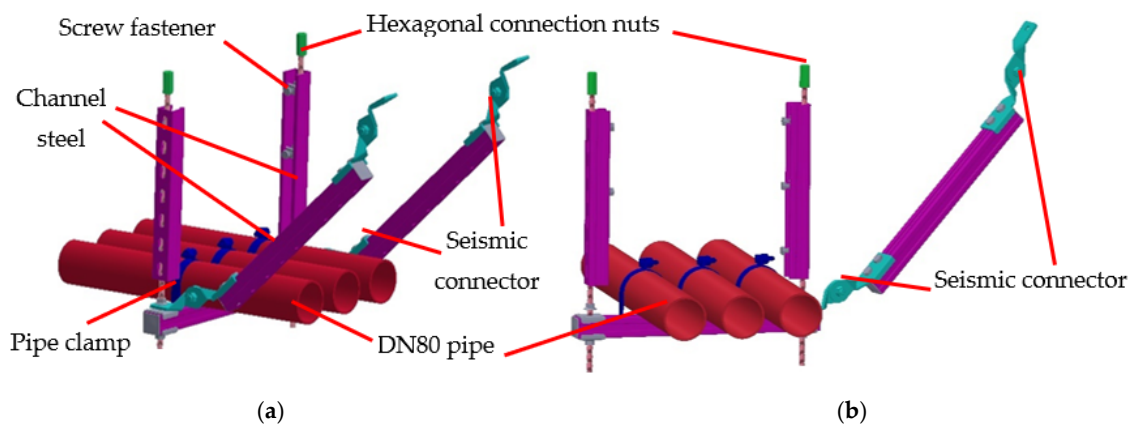


Figure 5. Test specimen of M2. (a) Test specimen of M2-X; (b) test specimen of M2-Y.

3. Test Protocol and Experimental Setup

3.1. Loading Protocol

The FEMA 461 [22] loading protocol loading strategy for seismic performance testing was used in this experiment. It is often adopted for evaluating displacement-dependent NSCs and identifying damage limit states. The loading protocol requires a minimum of ten loading scenarios, each of which must be executed twice. Before damage occurs, the specimen must be loaded for a minimum of six cycles, or three cases, with the displacement amplitude rising with each case. In addition, the loading amplitude of the last test should

be 1.4 times that of the first case. Typically, a monotonic static loading test is conducted to determine the maximum magnitude and displacement at the site of most damage. Figure 6 depicts the loading history, and the actuator loading speed is adjusted between 0.5 and 1 mm/s.

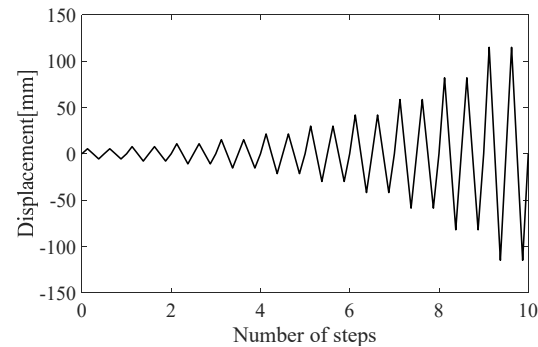


Figure 6. Typical testing protocol suggested by FEMA 461.

3.2. Experimental Setup

The experimental apparatus depicted in Figure 7 of this work was constructed using laboratory equipment. The quasi-static loading frame is the main component of the experiment, allowing for a good experimental design. The upper portion of a $1000 \times 800 \times 30$ mm steel plate features a total of six openings. Figure 6 depicts in light blue the components for the length of the 1500 mm M36 screw, whose end is fixed on a $1700 \times 1300 \times 12$ mm steel plate. This screw connects the upper steel plate to the frame's quasi-static load-bearing structure. The lower steel plate is pre-drilled, and the seismic bracing specimen is mounted on the lower steel plate. Meanwhile, the upper 30 mm thick steel plate was welded together with four $100 \text{ mm} \times 100 \text{ mm} \times 8 \text{ mm}$ square steel specimens to ensure that the overall stiffness of the experimental setup could meet the test requirements. The seismic bracing specimen is attached to the bottom steel plate, which is pre-drilled. Four $100 \times 50 \times 8$ mm channels connect to the loading frame's four columns to provide horizontal stiffness. It should be noted that the test is significantly impacted by the weight of the loading head of the actuator. This study combines a lifting rail and a self-balancing device to ensure that the loading actuator is always launched in a horizontal position, making the test as realistic as possible.

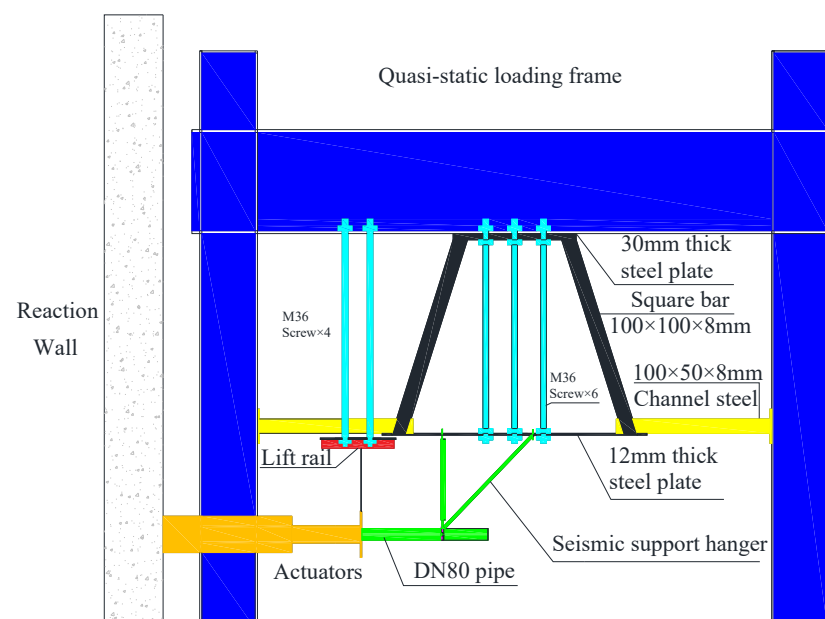


Figure 7. Experimental setup.

4. Test Result

Due to the diverse types of specimens tested in this study, this chapter will provide a detailed introduction to S1–X type specimens, while the other specimens will only be briefly described for significant phenomena.

4.1. S1 Test Specimen

According to the code of “Dimensions, shapes, masses, and tolerances of seamless steel tubes” [23], the nominal diameter of the DN 80 uninsulated pipe in the test should be 80 mm, and the outside diameter should be 89 mm. Due to the overall stiffness of the seismic bracing, the S1–X monotonic loading specimen was required primarily to reduce friction between the pipe and the pipe clamp. The force increased fast between 0 and 25 mm of loading displacement, although the diagonal brace showed no obvious deformation. As the pipe’s displacement increased, the component’s force remained practically constant at 2.4 kN. This type of seismic bracing was unable to arrest the pipe’s movement despite the fact that the component incurred no obvious damage.

The connection of the pipe clamp to the pipe are weak spots for the S1–X component when subjected to ground motion. Due to its significant stiffness, the seismic bracing diagonal brace of the S1–X fails first. To avoid this issue, the transmission line should be strengthened, for example, by reducing the rigidity of the S1–X component diagonal brace so that it can aid in the dissipation of energy during an earthquake. In this study, the S1–X specimen was used to examine the hysteresis performance and damage process of this type of seismic bracing without considering the effect of pipe clamps. Figure 8 depicts the installation diagram of the specimen.

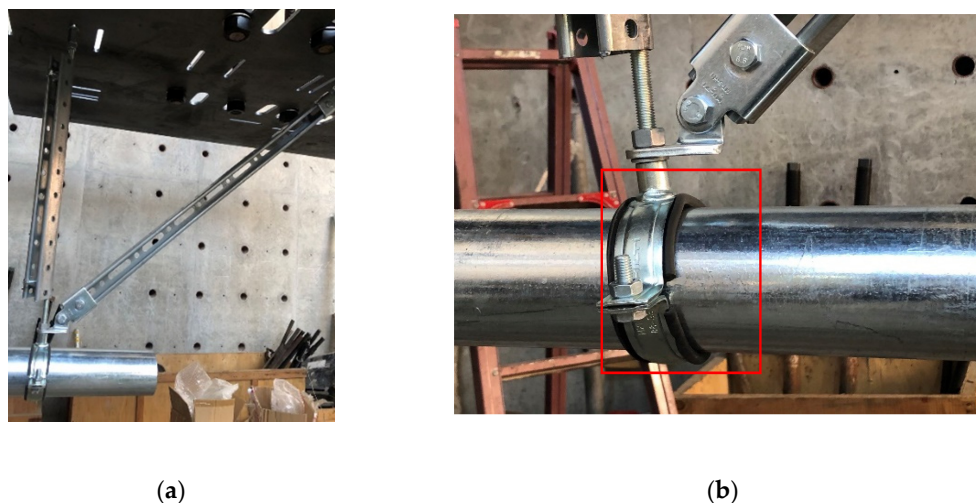


Figure 8. S1–X specimen with tube clamp. (a) Test specimen installation; (b) failure of pipe clamp connection.

To investigate the hysteresis behavior and failure modes of the seismic bracing, the S1–X specimen in the following text does not consider the influence of the pipe clamp, and the specimen of this type is studied. The installation diagram of the specimen is shown in Figure 9. The displacement amplitude of the test loading is determined based on the monotonic loading test, and in this paper, the displacement amplitude is defined as the displacement value corresponding to 0.85 times the peak force after the peak force.

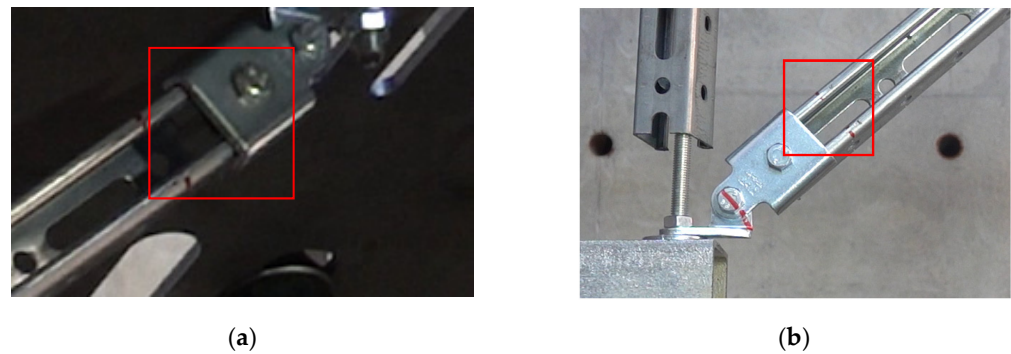


Figure 9. S1–X specimen test pictures without tube clamp. (a) Upper seismic connector pull–out; (b) lower seismic connector pull–out.

The maximum force of specimen 1 (numbered S1–X–C–1) (Figure 10a) in the cyclic loading test was 12.89 kN and -7.94 kN, respectively. Additionally, the type of seismic bracing was primarily dissipated through the sliding of the torsional shear clips in the diagonal brace. When the loading displacement reached 40.92 mm, the upper torsional shear clip in the diagonal brace was nearly ripped out, and the test was terminated due to the severe loss in bearing capacity. As the loading displacement rose in the following cases, the relative displacement of the upper torsional shear clip and diagonal brace channel steel gradually increased. The test of specimen S1–X–C–2 (Figure 10b) was terminated at 40.92 mm when the diagonal brace’s torsional shear clip nearly came undone. When S1–X–C–3 (Figure 10c) was loaded to 56.52 mm, the specimen was damaged and the seismic connector was split from the channel steel.

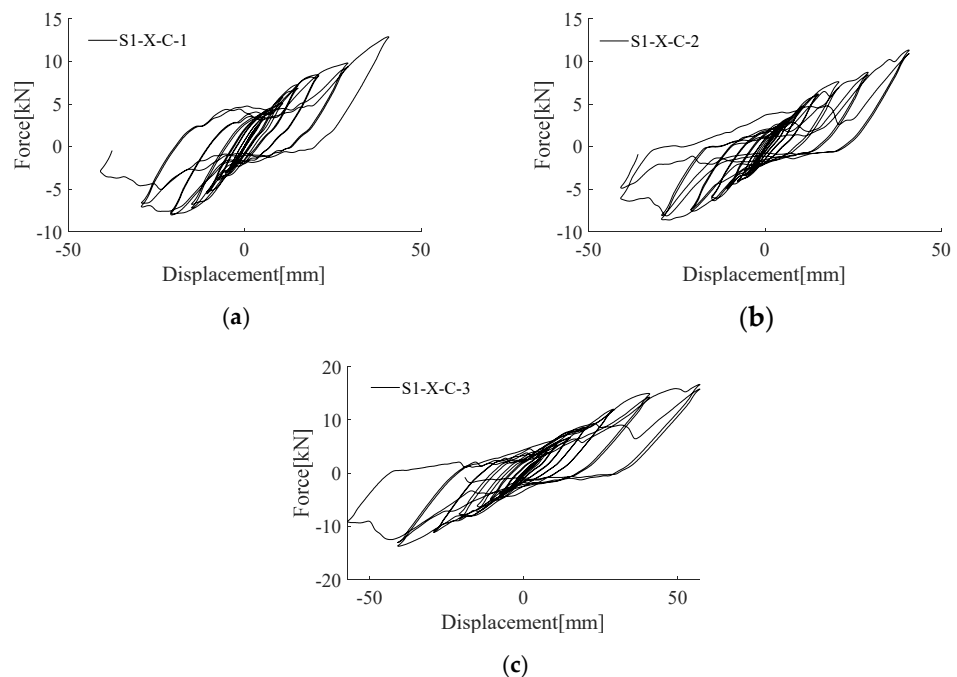


Figure 10. Hysteresis curve of S1–X specimens without the tube clamp. (a) S1–X–C–1; (b) S1–X–C–2; and (c) S1–X–C–3.

The installation sizes of the three groups of specimens were identical, and the torsional shear clip of each group met the minimum requirement of $40 \text{ N}\cdot\text{m}$. The three groups of specimens indicated three separate types of damage, but it was evident that combining both the upper and lower seismic connections in energy dissipation at the same time could greatly boost the seismic bracing carrying capacity.

Specimen S1–Y was subjected to quasi–static loading with a displacement amplitude of 165.7 mm. Three cyclic tests were conducted on S1–Y. In the cyclic loading test, the positive and negative peak forces for specimen 1 were 8.15 kN and -7.38 kN, respectively. When the loading displacement was between 0–22.01 mm, the deformation mainly occurred in the pipe clamp. There was slight sliding in the upper seismic connector. At the second cycle of the 83.16 mm, the load–carrying capacity was basically lost. During the 118.36 mm loading condition, the threaded rod in the lower vertical suspension support fractured, and the test ended. The test phenomena of S1–Y–C–2 and S1–Y–C–3 are similar to S1–Y–C–1.

The test photos and hysteresis curve of the specimens are shown in Figures 11 and A1, respectively.

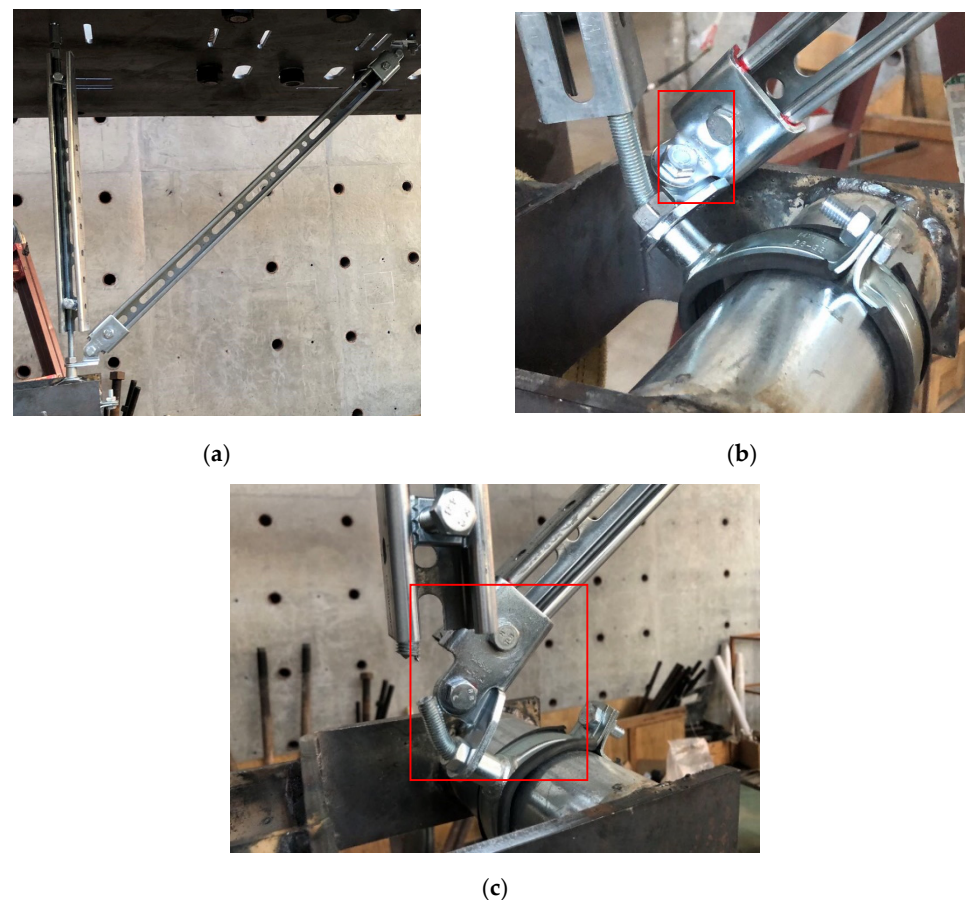


Figure 11. S1–Y specimen test pictures. (a) Test specimen installation; (b) buckling of seismic connectors in cycling test; and (c) screw breakage in cycling test.

4.2. S2 Test Specimen

The clamp of the S2–X specimen does not provide basic restraining capability. Therefore, in this section, the clamp is removed for quasi–static tests of the specimen, with a quasi–static loading amplitude of 61.89 mm.

Three sets of cyclic tests were conducted on the S2–X specimen. For specimen 1, the peak positive and negative forces were 4.24 kN and -4.40 kN, respectively. When the displacement reached 16.1 mm, the upper seismic connector buckled, then the lower seismic connector began to buckle, and its deformation continued to increase in subsequent cases. Significant relative sliding occurred between the torsional shear clip of the upper seismic connector and the channel steel of the diagonal brace. At the 22.9 mm case, the pre–tensioned bolt rotated, the lower seismic connector underwent significant deformation, and it contacted the suspended support channel steel, which increased its bearing capacity.

The lower part of the suspended support began to buckle and absorb energy, and the lower seismic connector underwent slight sliding. Finally, the lower seismic connector underwent out-of-plane bending, and the test ended. The test phenomena of S2-Y-C-2 and S2-Y-C-3 were similar to S2-Y-C-1, the difference is the torsional shear clip of the lower connector was pulled out, and specimen S2-Y-C-3 was destroyed.

The test photos and hysteresis curve of the specimens are shown in Figures 12 and A2, respectively.

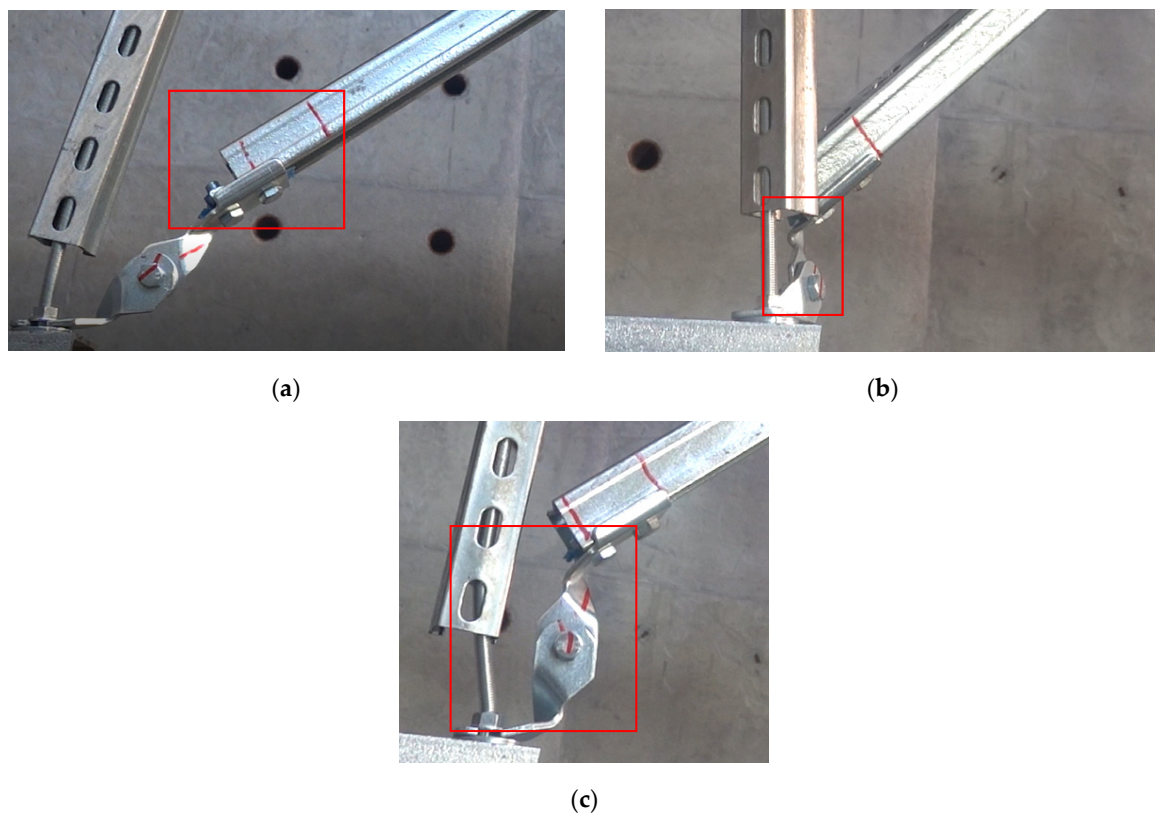


Figure 12. S2-X specimen test pictures. (a) Seismic connectors come out during monotonic loading test; (b) out-of-plane buckling of seismic connectors in cycling test; and (c) buckling of seismic connector and screw in cycling test.

The quasi-static loading amplitude for specimen S2-Y is 74.46 mm. During the cyclic loading test, the maximum force of specimen 1 (S2-Y-C-1) was 3.03 kN and -4.26 kN, respectively. The pipe clamp distorted the greatest between 0 and 10 mm of loading displacement. Upper and lower seismic connectors exhibited flexural deformation as the loaded displacement increased. When the loaded displacement reached 27 mm, the vertical suspension support in the lower screw exhibited plastic deformation. During the test, the lower seismic connectors and pipe clamps that contacted the position of the lower connector slowly pulled out. The test was terminated once the bottom connector and pipe clamps at the screw were removed. Specimen 2 (S2-Y-C-2) had a maximum force of 2.80 kN, -4.58 kN, whereas specimen 3 (S2-Y-C-3) exhibited a maximum force of 2.39 kN, -4.47 kN. Comparing specimen 1 (S2-Y-C-1) to specimen 2 (S2-Y-C-2), the specimens did not demonstrate the same lower connection failure and screw connection failure.

The test photos and hysteresis curves of the specimens are shown in Figures 13 and A3, respectively.

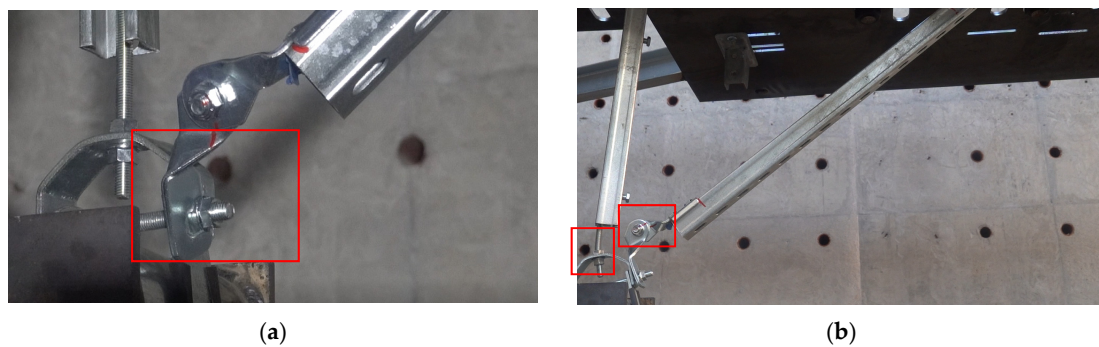


Figure 13. S2–Y specimen test pictures. (a) The seismic connector comes out; (b) seismic connectors and screw buckling.

4.3. M1 Test Specimen

The M1–X specimen is a three–pipe seismic bracing, similar to the S1–X specimen. During monotonic loading tests, when the displacement reached 36 mm, the force remained basically constant at 6.3 kN as the displacement increased. Although the entire system did not fail, this type of seismic bracing was unable to limit the pipe displacement. In order to investigate the hysteretic performance and failure mode of this type of seismic bracing system, the influence of the clamp on the M1–X specimen is not considered in the quasi–static loading tests, and the displacement amplitude is set to 69.57 mm.

Three cyclic loading tests were performed on the M1–X specimen. In the cyclic loading tests, the peak positive and negative forces of specimen 1 were 22.59 kN and -24.08 kN, respectively. When the loading reached 35.72 mm, a significant rotation occurred at the hinge of the lower seismic connector. When the displacement reached 50.22 mm, the lower seismic connector on one side buckled and failed, and the test was terminated. Before the 50.22 mm case, the test phenomena of M1–X–C–2 and M1–X–C–3 were basically the same as that of M1–X–C–1; however, M1–X–C–2 and M1–X–C–3 both failed in the 69.57 mm case.

The test photos and hysteresis curves of the specimens are shown in Figures 14 and A4, respectively.

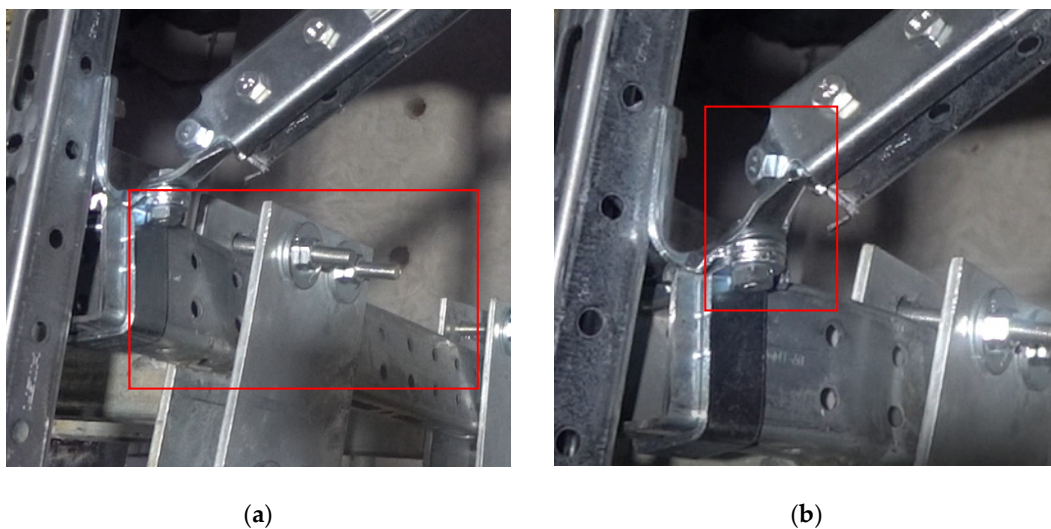


Figure 14. M1–X specimen test pictures. (a) Channel buckling; (b) buckling of seismic connector.

The quasi–static amplitude of the M1–Y specimen is 73.13 mm. The peak forces of specimen 1 in the positive and negative directions were 10.82 kN and -13.44 kN, respectively. When the loading displacement was 0–19.04 mm, the deformation mainly occurred in the pipe clamp. As the loading displacement increased, in the 26.7 mm loading

case, the torsional shear clip began to slide, and the pre-tensioned bolts of the lower seismic connector began to rotate. In the 52.3 mm case, the pipe clamp underwent severe deformation. When loaded to 73.13 mm, the seismic connector of the lower part of the diagonal brace buckled and bent out of plane, and the test ended. The test phenomena of the last two sets of specimens were basically the same as that of M1–Y–C–1, and all resulted in the buckling of the seismic connector in the diagonal brace, causing a decrease in bearing capacity.

The test photos and hysteresis curves of the specimens are shown in Figures 15 and A5, respectively.

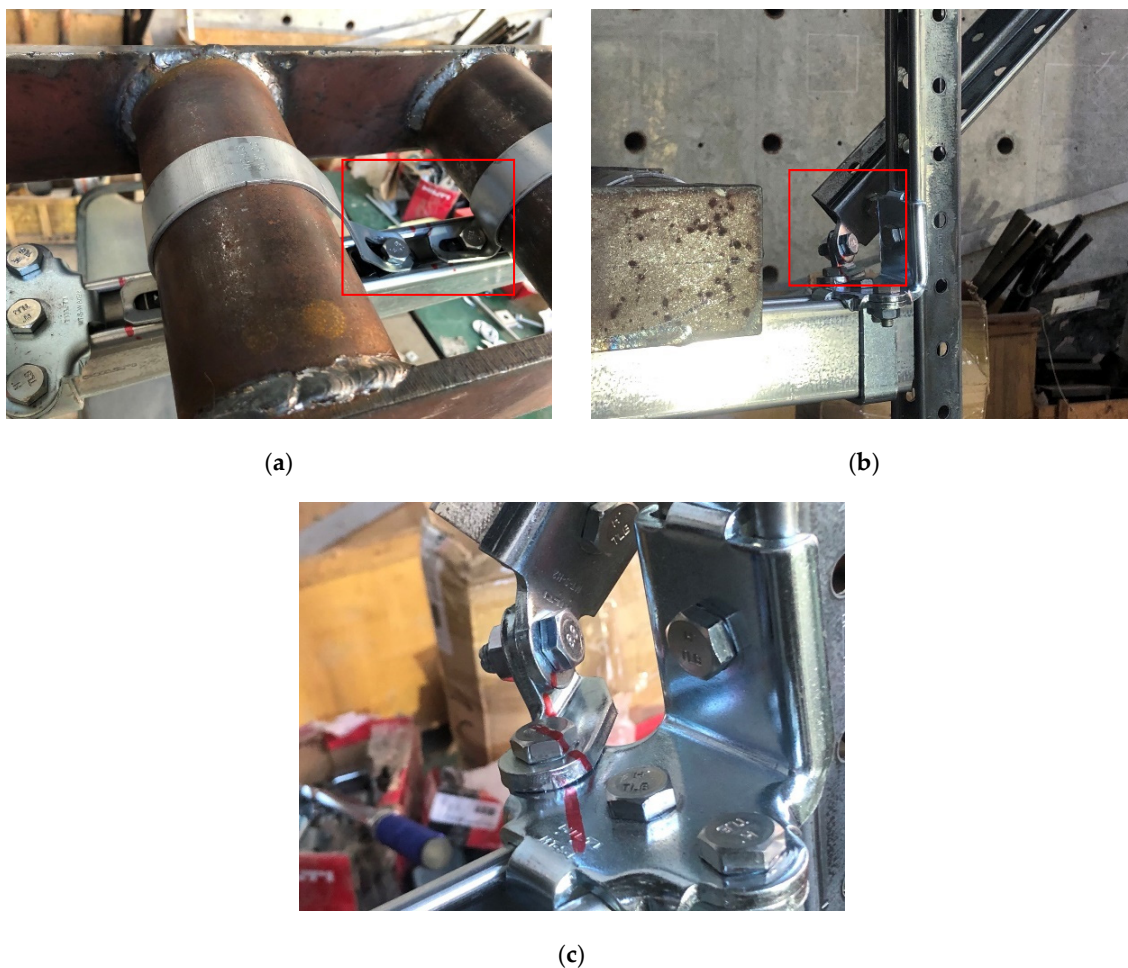


Figure 15. M1–Y specimen test pictures. (a) Pipe clamp damage; (b) buckling of the seismic connector; and (c) detail of the damage to the seismic connector.

4.4. M2 Test Specimen

The quasi-static loading displacement amplitude of M2–X is 155.0 mm. Three cyclic tests were conducted on M2–X. For M2–X–C–1, the peak positive and negative forces were 8.68 kN and -9.67 kN, respectively. At the beginning of the test, all parts except for the lower seismic connector began to cooperate to dissipate energy. As the displacement increased, the upper seismic connector and the horizontal channel steel deformed more and more. When loaded to 40.4 mm, the lower seismic connector began to yield and dissipate energy. In the next test cycle (56.5 mm), the pre-tensioned bolt of the lower seismic connector started to rotate and undergo significant deformation, while the torsional shear clip of the upper seismic connector and the channel steel underwent minor relative deformation. Finally, the specimen failed at the 155 mm displacement case, with the pipe

and clamp connection failing and the bearing capacity rapidly decreasing. Significant permanent deformation of the horizontal channel steel was observed during the test.

For the specimens M2–X–C–2 and M2–X–C–3, the test phenomena were basically the same as that of M2–X–C–1. Figure 16 displays the photograph of the specimen during the test, and Figure A6 shows the hysteresis curve of the specimen.

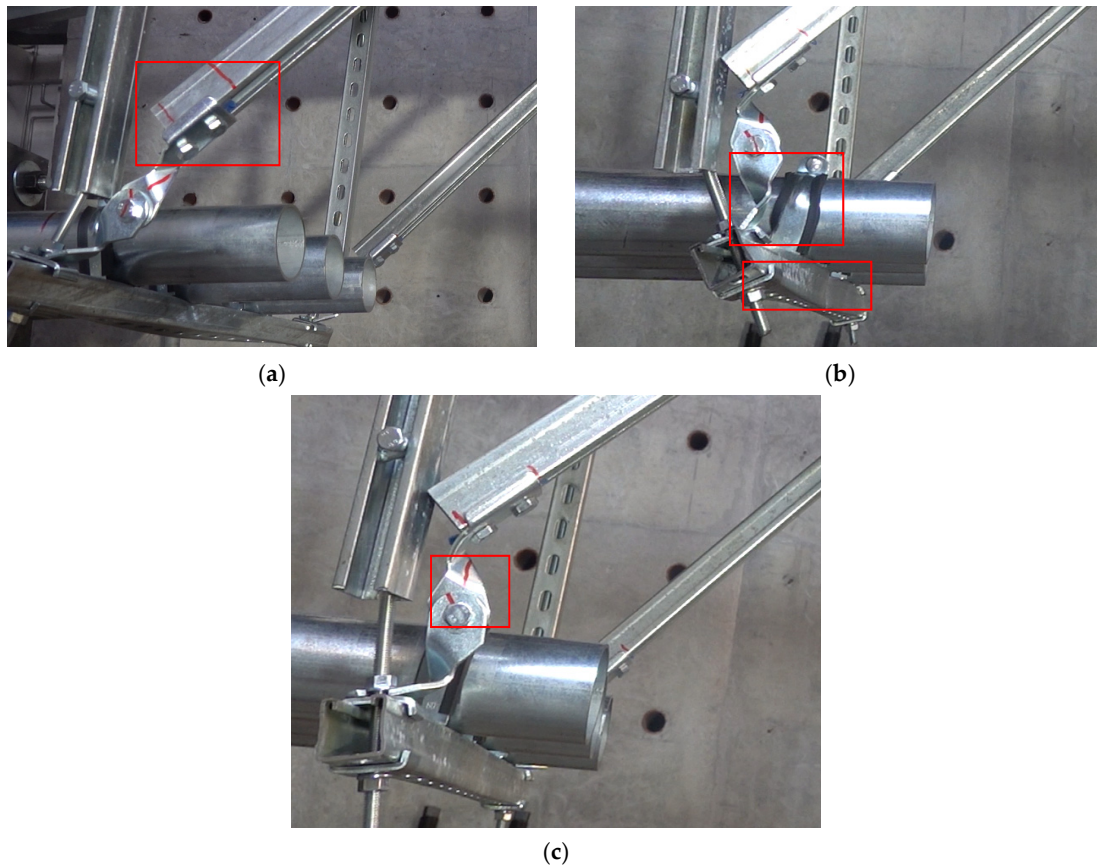


Figure 16. M2–X specimen test pictures. (a) Failure of connection between the seismic connector and the diagonal brace; (b) failure of the connection between the pipe clamp and the pipe and buckling of the horizontal channel steel; and (c) pre-tightening bolt rotation.

The M2–Y test specimen was subjected to quasi-static test with a displacement amplitude of 135 mm. The maximum positive and negative peak loads for specimen 1 were 5.63 kN and –5.90 kN, respectively. When the loading displacement was 0–17.9 mm, the main energy dissipation was due to the deformation of the pipe clamp and the buckling of the upper seismic connector. At the loading case of 25.1 mm, the upper part of the channel steel in the diagonal brace contacted the top steel plate, and the lower seismic connector began to undergo small deformation. At the loading case of 68.88 mm, the lower seismic connector had undergone significant deformation and began to undergo out-of-plane bending, and the bearing capacity started to decrease. Finally, at the loading case of 96.4 mm, the lower seismic connector disconnected from the vertical suspension support screw, and the specimen was destroyed, ending the test.

The test phenomena for the last two groups of specimens were different from that of M2–Y–C–1. For M2–Y–C–1, the out-of-plane displacement of the lower seismic connector occurred at 68.88 mm; however, for M2–Y–C–2 and M2–Y–C–3, buckling and decreased bearing capacity occurred when loaded to 49 mm.

The test photos and hysteresis curves for the specimens are shown in Figures 17 and A7, respectively.

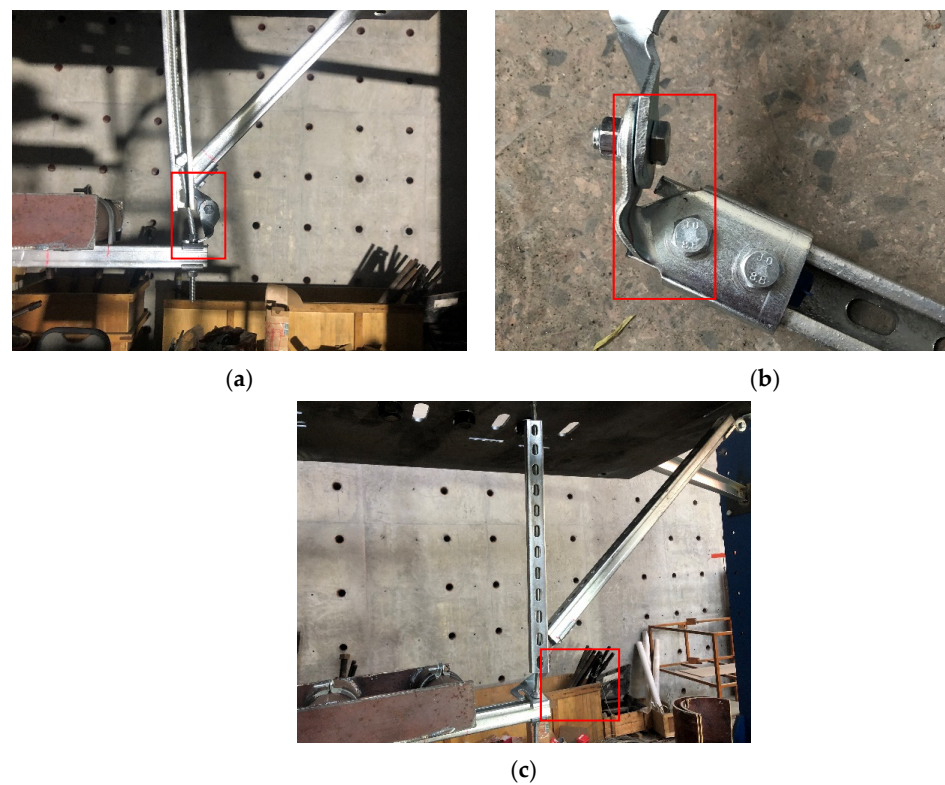


Figure 17. M2–Y specimen test pictures. (a) Buckling of seismic connector; (b) damage of seismic connector; and (c) the seismic connector comes out.

5. Seismic Performance Comparison of Various Specimens

NSC seismic design, as one of the important research topics in the field of scientific and integrated sustainable development, can ensure the functionality of building structures during natural disasters such as earthquakes, thereby safeguarding people’s lives and property and contributing to post–earthquake seismic relief efforts. Seismic research on NSCs is important to human sustainable development. The water supply pipeline system, as an important NSC, plays a significant role in ensuring the integrity of building functionality. The following experimental results were discussed and analyzed.

5.1. Fragility Theory

Fragility refers to the likelihood that a component or system would suffer damage beyond a predetermined damage state when exposed to seismic events of varied intensities. Typically, this probability is assumed to follow a log–normal distribution. The FEMA P–58 [24] document describes the specific methodology of fragility analysis. Fragility function can be expressed as:

$$F(\mu) = \Phi\left(\frac{\ln\left(\frac{\mu}{\mu_m}\right)}{\beta}\right) \quad (1)$$

where Φ is the cumulative function of the standard normal distribution; m is the number of specimens. μ_m and β are calculated using Equations (2) and (3), respectively:

$$\mu_m = e^{\frac{1}{M} \sum_{i=1}^M \ln \mu_i} \quad (2)$$

$$\beta = \sqrt{\frac{1}{M-1} \sum_{i=1}^M \left(\ln\left(\frac{\mu_i}{\mu_m}\right)\right)^2 + \beta_u^2} \quad (3)$$

where μ_m and β are the mean value of engineering demand parameters (EDPs) and its logarithmic standard deviation, respectively. M is the total number of specimens considered. i represents the sample number. μ_i is the specific value of the EDPs associated with the damage of specimen i . β_u is the correction factor of β , which can be assumed to equal 0.25 if all specimens have the same loading process.

5.2. Engineering Demand Parameters

It is generally important to specify a variety of EDPs to aid in the performance-based design and seismic hazard evaluation of NSCs. On the basis of the structural component theory of the Standard for Seismic Test of Buildings JGJ/T 101–1996 [25], the EDPs can be calibrated using monotonic and cyclic loading tests of seismic bracing.

In the previous literature, some scholars used the ductility factor as an engineering demand parameter to calculate the fragility of pipeline systems. Whereas the ductility factor usually indicates the deformation capacity of the system, and the bearing capacity which is closely related to the performance of the pipeline systems was not considered. In order to simultaneously improve the bearing capacity and deformation capacity of the seismic bracing, this study selects the area under the cyclic envelope at a displacement value in the cyclic test (E , shown in Figure 18) as the engineering demand parameter for seismic bracing. The GB 50011–2010 code [26] highlights that the seismic fortification objectives of non-structural components are coordinated with the three-level fortification objectives of the main structure, allowing the damage of non-structural components of the building to be slightly greater than the main structure but not life-threatening. The three-level fortification objectives are, respectively, “frequent earthquake is not damage, fortification earthquake is repairable, and rare earthquake is not collapse”. Therefore, the component can be divided into three damage levels, which correspond to the three performance objectives in the specification.

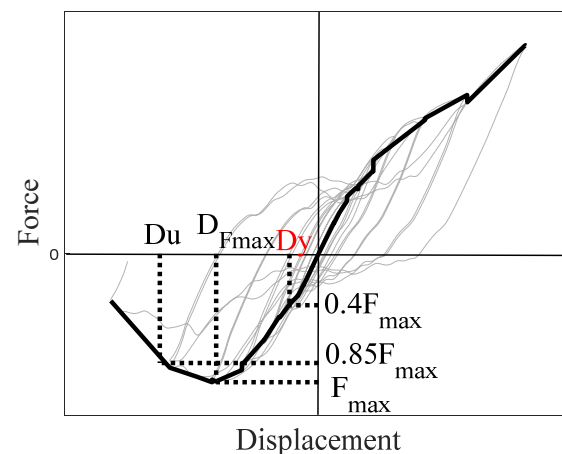


Figure 18. Calculation method used to determine the energy values.

(1) The components basically remain elastic without damage. Since JGJ/T 101–1996 (1997) defines cracks in concrete as the beginning of the specimen to enter the yield state, which obviously does not apply to non-structural components, this article quotes FEMA P–795 (2011) to define the displacement value corresponding to the first reaching 0.4 times of the peak force as the yield displacement D_y , and the corresponding component envelope curve area at the yield displacement is related to DL 1 (damage level). The corresponding EDPs is E_1 .

(2) The component is partially elastic–plastic, but can be repaired by replacing accessories. Generally, in the cyclic loading test, when the test piece reaches the peak force, the existing fittings in the component appear partially elastic–plastic, so the displacement value corresponding to the peak force (D_{Fmax}) is taken as the key parameter to evaluate whether the test specimen reaches DL 2. The corresponding EDPs is E_2 .

(3) The reduced bearing capacity of the components can not completely guarantee the safety of human life. According to JGJ/T 101–1996, when the bearing capacity of the component is reduced to 0.85 times of the peak force, it is judged that the member is seriously damaged. Therefore, the deformation corresponding to 0.85 F_{max} within the range after the peak value can be defined as the ultimate displacement D_u . By determining the displacement value, the corresponding energy value can be solved. The corresponding EDPs is E_3 .

Because the envelope curve contains positive peak force and negative peak force, the smaller of the absolute value of the peak force is taken as the actual bearing capacity of the component in this paper. The yield displacement, the displacement corresponding to the peak force, and the ultimate displacement mentioned above all correspond to the actual bearing capacity area of the component.

5.3. Fragility of Test Specimens

In this section, the fragility of various specimens to damage will be studied using the EDP determined in the previous section.

For example, the fragility study of S1–X was conducted in accordance with the FEMA P58 fragility theory, with the resulting engineering criteria listed in Table 2. As mentioned in Section 5.2, if the performance objective of “no damage in frequent earthquake” is attained, the energy value is 15.90 J. Similarly, if the performance objective of “repairable in fortification earthquake” and “no collapse in the rare earthquake” are attained, the energy values are 165.07 J and 275.55 J, respectively. Figure 19d demonstrates the relationship between energy and the probability of exceeding the energy capacity.

Table 2. Parameters of the response of S1.

Number	Specimen	Loading Category	F_{max} [kN]	D_y [mm]	D_{Fmax} [mm]	D_L [mm]	E_1	E_2	E_3
1	S1–X	Monotonic	13.63	15.23	54.82	56.53	–	–	–
2		Cyclic	12.89 –7.94	10.78 –5.74	40.70 –21.04	– –30.16	10.14	95.72	177.33
3		Cyclic	11.33 –8.61	10.17 –5.75	40.73 –27.24	– –37.19	10.29	145.69	223.93
4		Cyclic	16.66 –13.72	14.94 –12.00	57.13 –40.68	– –49.55	38.52	322.57	430.21
5	S1–Y	Monotonic	–10.49	–45.90	–145.6	–163.6	–	–	–
6		Cyclic	8.15 –7.38	24.86 –20.66	135.51 –116.44	139.03 –	49.21	577.25	611.73
7		Cyclic	5.95 –8.92	7.79 –14.89	106.50 –82.92	107.42 –	9.33	390.78	397.24
8		Cyclic	8.49 –11.50	19.83 –33.33	116.17 –114.80	116.17 –	41.60	570.79	570.79

The peak force parameters of the S1 specimens are shown in Table 2, and the fragility calculation parameters are shown in Table 3 (E_m are the mean value of engineering demand parameters). The peak force parameters of the S2, M1, and M2 specimens are shown in Tables 4–6, with fragility parameters shown in Table 3. The fragility curves of specimens S1–X to M2–Y are shown in Figure 19a–h.

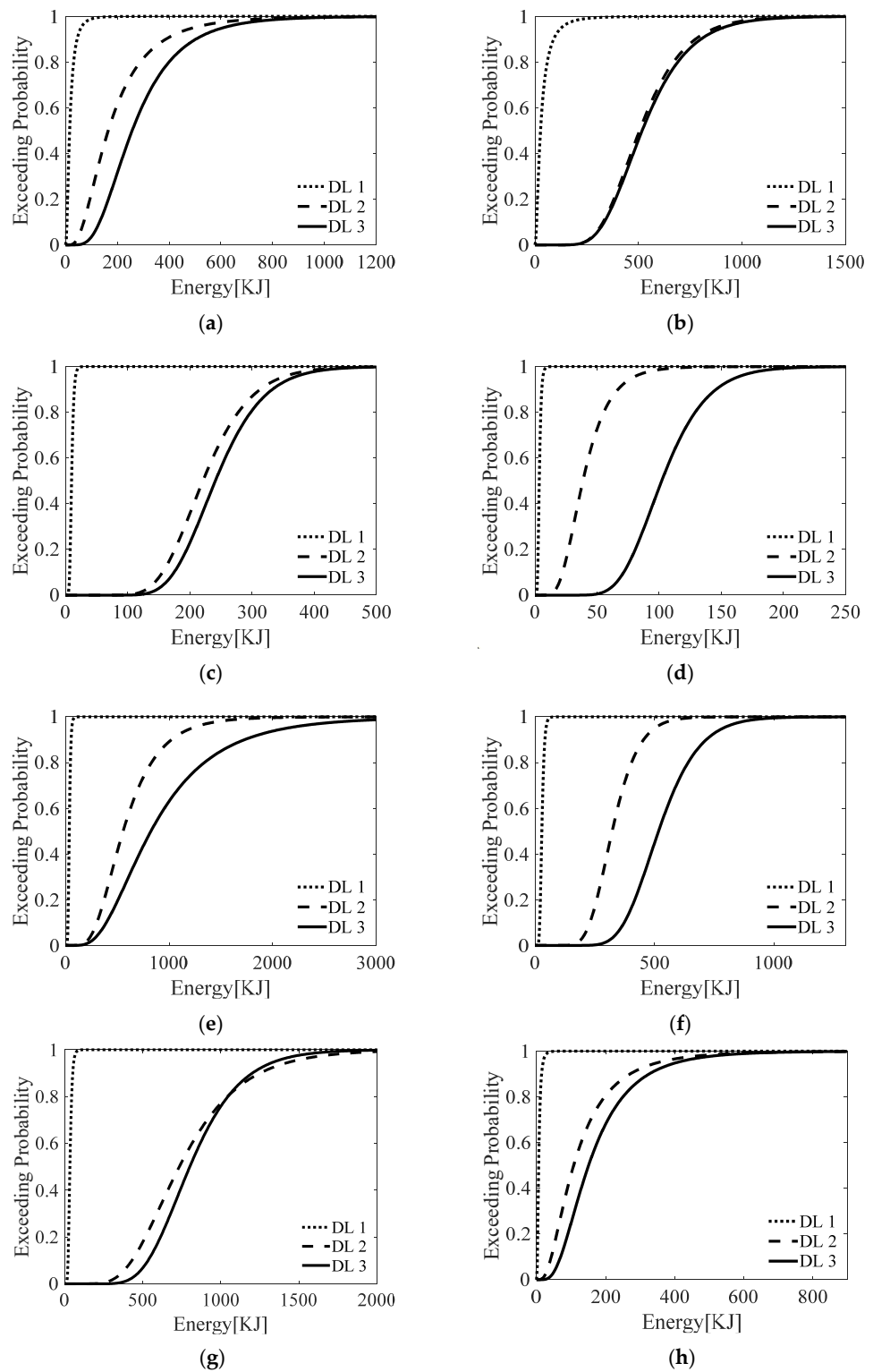


Figure 19. Fragility of test specimens. (a) S1–X; (b) S1–Y; (c) S2–X; (d) S2–Y; (e) M1–X; (f) M1–Y; (g) M2–X; and (h) M2–Y.

Table 3. Parameters of fragility analysis.

Type of Specimen	DL 1		DL 2		DL 3	
	E_m	β	E_m	β	E_m	β
S1–X	15.90	0.81	165.07	0.67	257.55	0.52
S1–Y	26.74	0.95	504.96	0.33	517.64	0.34
S2–X	9.72	0.30	221.22	0.27	241.23	0.25
S2–Y	3.45	0.36	38.57	0.43	102.02	0.28
M1–X	36.10	0.31	556.70	0.48	825.43	0.58
M1–Y	28.68	0.29	323.21	0.27	517.37	0.25
M2–X	33.83	0.34	733.86	0.42	801.12	0.32
M2–Y	6.11	0.68	107.55	0.72	150.85	0.60

Table 4. Parameters of the response of S2.

Number	Specimen	Loading Category	F_{max} [kN]	D_y [mm]	D_{Fmax} [mm]	D_L [mm]	E_1	E_2	E_3
1	S2–X	Monotonic	−6.63	−14.78	−59.91	−61.79	—	—	—
2		Cyclic	4.24	6.32	44.27	58.96	8.70	202.45	236.45
3		Cyclic	−5.4	−7.84	−55.65	−62.22	9.02	248.88	248.88
4		Cyclic	5.26	9.60	61.85	62.21	—	—	—
5	S2–Y	Monotonic	−5.71	−7.88	−62.15	—	11.71	214.86	238.55
6		Cyclic	5.67	7.17	61.38	—	—	—	—
7		Cyclic	−5.88	−9.33	−57.08	−60.4	—	—	—
8		Cyclic	−4.79	−13.71	−65.84	−74.66	4.63	51.49	88.67
1	S2–Y	Monotonic	3.03	7.98	27.2	37.81	—	—	—
2		Cyclic	−4.26	−9.18	−53.62	—	3.10	42.53	108.18
3		Cyclic	2.8	7.92	24.88	40.26	—	—	—
4		Cyclic	−4.58	−10.69	−62.99	−69.23	2.87	26.21	110.68
5	S2–Y	Monotonic	2.39	7.04	19.1	54.96	—	—	—
6		Cyclic	−4.47	−8.84	−53.54	−59.95	—	—	—
7		Cyclic	—	—	—	—	—	—	—
8		Cyclic	—	—	—	—	—	—	—

Table 5. Parameters of the response of M1.

Number	Specimen	Loading Category	F_{max} [kN]	D_y [mm]	D_{Fmax} [mm]	D_L [mm]	E_1	E_2	E_3
1	M1–X	Monotonic	27.11	8.93	36.08	70.27	—	—	—
2		Cyclic	22.59	6.70	31.63	50.21	31.27	484.39	484.39
3		Cyclic	−24.08	−8.72	−35.9	−45.65	44.69	877.66	1368.72
4		Cyclic	28.16	7.83	44.13	59.5	33.67	405.82	848.25
5	M1–Y	Monotonic	−25.09	−8.89	−44.52	−49.95	—	—	—
6		Cyclic	21.56	8.44	30.9	50.85	33.51	350.89	534.37
7		Cyclic	−24.07	−9.90	−35.71	−48.28	27.29	293.37	490.23
8		Cyclic	13.72	17.24	72.01	73.13	25.80	327.99	528.63
1	M1–Y	Monotonic	10.82	13.70	57.31	74.96	—	—	—
2		Cyclic	−13.44	−21.83	−75.03	—	—	—	—
3		Cyclic	9.37	13.12	53.36	74.96	—	—	—
4		Cyclic	−12.67	−18.65	−74.99	—	—	—	—
5	M1–Y	Monotonic	10.06	11.94	53.11	74.13	—	—	—
6		Cyclic	−11.29	−15.66	−58.96	−75.27	—	—	—
7		Cyclic	—	—	—	—	—	—	—
8		Cyclic	—	—	—	—	—	—	—

Table 6. Parameters of the response of M2.

Number	Specimen	Loading Category	F_{max} [kN]	D_y [mm]	D_{Fmax} [mm]	D_L [mm]	E_1	E_2	E_3
1	M2–X	Monotonic	–11.98	–19.30	–141.7	–155.1	–	–	–
2		Cyclic	8.68	11.86	109.43	–	27.46	507.94	658.35
3		Cyclic	–9.67	–18.87	–75.97	–91.93	42.89	969.38	969.38
4		Cyclic	10.2	9.79	153.69	–	32.87	802.67	805.64
			–11.5	–16.93	–121.57	–155.1			
			9.09	22.85	146.45	–			
			–10.36	–14.61	–109.95	–110.1			
5	M2–Y	Monotonic	–7.6	–30.78	–125.1	–135	–	–	–
6		Cyclic	5.63	10.35	68.85	75.87	12.58	234.91	283.10
7		Cyclic	–5.9	–12.75	–96.3	–	3.93	71.84	116.47
8		Cyclic	3.13	6.36	33.88	49.24	4.62	73.71	104.10
			–4.98	–16.69	–68.84	–96.69			
			3.53	6.63	34.39	41.56			
			–7.89	–14.58	–131.41	–			

5.4. Performance of Various Specimens

According to the test information obtained above, this section summarizes and evaluates the bearing capacity of the above types of test specimens, the engineering demand parameters corresponding to each damage level, the damage mode of the components, and the evaluation of the components (Table 7). Finally, the disadvantages of various test specimens in the test are analyzed and some suggestions for improvement are put forward.

For example, the bearing capacities of the S1–Y and S2–Y specimens are far greater than that of the S2–Y specimens. When the damage state of the component reaches DL 1, the corresponding engineering demand parameters of S1–Y and S2–Y specimens are 26.74 J and 3.45 J, respectively. It can be seen that the performance of the S1–Y specimens is much better than that of the S2–Y specimens. The bearing capacity of the S2–Y test specimen is too low and the seismic connector can easily fall off.

The above table summarizes the bearing capacity and deformation capacity of various test specimens, and analyzes the advantages and disadvantages of various test specimens. The following improvement suggestions are proposed to address the problems exposed by the test results:

(1) For the S1–X and M1–X specimens, the seismic bracing itself has a strong bearing capacity, but the connection between the pipes and the pipe clamp is weak and is very easy to damage. Therefore, it should be strengthened by improving the connection strength between the pipe clamp and the pipe.

(2) For the S2–X specimens, due to design defects, the restraint capacity of the pipeline is basically absent. To solve this problem, the solution shown in the Figure 20 is proposed in this paper.

(3) S2–Y, M2–X, and M2–Y specimens exposed the problem of low initial stiffness of seismic connections in the test, resulting in lower bearing capacity than the S1 and M1 specimens. The hinges in the seismic connections used in the S2 and M2 specimens form an angle by themselves. Long distances may cause the pre-tensioned bolts in the seismic connector to rotate very easily and lead to the specimens being prone to out-of-plane deformation, which leads to further damage to the specimens. It is recommended that seismic connections be shortened and made appropriately thicker. Secondly, the gap between the lower seismic connector and the pipe clamp or the screw connection can easily lead to the separation of the seismic connector from the vertical suspension. It is recommended that this gap be eliminated.

Table 7. Summary of performance parameters of various test specimens.

Type of Specimen	Mean of Peak Force (kN)	Damage Level	Logarithmic Mean of EDP (J)	Description of Damage	Evaluation of Specimens
S1–X	10.09	DL 1	15.90	Suspended screw with slight deformation	The seismic bracing has strong bearing capacity, but the connection between the pipe clamp and the pipe is easily damaged
		DL 2	165.07	Suspended screw with plastic deformation; seismic connector rotation	
		DL 3	257.55	Seismic connector pulls out from the channel steel	
S1–Y	7.27	DL 1	26.74	Suspended screw and pipe clamp with slight deformation	High bearing capacity and good ductility
		DL 2	504.96	Suspended screw with plastic deformation; seismic connector rotation	
		DL 3	517.64	Seismic connector damage; suspended screw breakage	
S2–X	5.06	DL 1	9.72	Seismic connector exhibits slight rotation; suspended screw with slight deformation	The design is unreasonable, and attention should be paid to restraining the lateral deformation of the pipeline
		DL 2	221.22	Seismic connector yield; large rotation of seismic connector; suspended screw yield	
		DL 3	241.23	Seismic connector pulls out from the channel steel; out-of-plane deformation of the seismic connector	
S2–Y	2.74	DL 1	3.45	Seismic connector rotates slightly; suspended screw with slight deformation	The bearing capacity is weak, and the seismic connector is easy to come out
		DL 2	38.57	Suspended screw with plastic deformation; seismic connector yield	
		DL 3	102.02	Connection of seismic connector and pipe clamp comes out; out-of-plane deformation of seismic connector	
M1–X	23.08	DL 1	36.10	Seismic connection kit exhibits slight deformation	The seismic bracing has strong bearing capacity, but the connection between the pipe clamp and the pipe is easily damaged
		DL 2	556.70	Yielding of the horizontal channel steel; slight rotation of the preload bolt in the seismic connector	
		DL 3	825.43	Seismic connector yield	
M1–Y	10.08	DL 1	28.68	Pipe clamp deformation	Acceptable bearing capacity
		DL 2	323.21	Significant deformation of the clamp	
		DL 3	517.37	Out-of-plane yielding of seismic connection; pipe clamp severely damaged	
M2–X	9.32	DL 1	33.83	Pipe clamp and suspended screw slightly deformed	The overall stiffness is relatively small, which is prone to large deformation
		DL 2	733.86	Suspended screw yielding; rotation of the preload bolt in the seismic connector	
		DL 3	801.12	Seismic connector pulls out from the channel steel; the pipe clamp loses its restraint ability	
M2–Y	4.10	DL 1	6.11	Pipe clamp and suspended screw slightly deformed	Low bearing capacity and easy to damage
		DL 2	107.55	Suspended screw yielding; rotation of the preload bolt in the seismic connector	
		DL 3	150.85	Out-of-plane yielding of seismic connection; pipe clamp severely damaged	

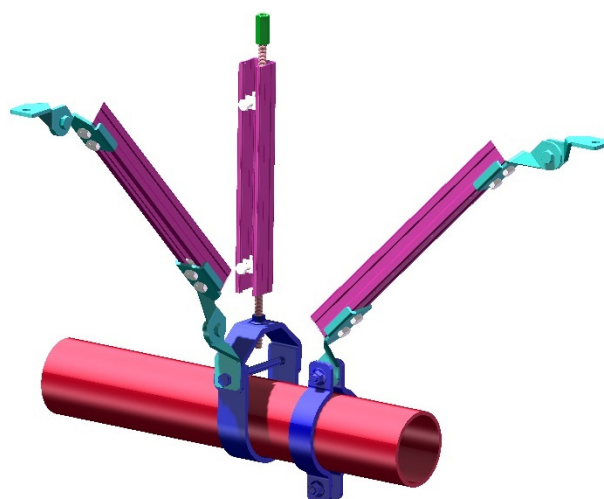


Figure 20. Improvement method.

6. Conclusions

This paper conducted a total of 34 sets of monotonic and cyclic loading tests on four types of seismic bracing systems in important buildings and analyzed the fragility of various seismic bracing types based on the test results. The conclusions obtained are as follows:

(1) Except for the S1–Y test specimen, other test specimens did not lose the vertical bearing capacity at the end of the test.

(2) Although some issues still exist in determining the engineering demand parameters (EDPs) for seismic bracing discussed in previous studies, this paper discusses the EDPs used in the pipeline system and takes the envelope area of the force and displacement envelope curve at a certain displacement value obtained from the cyclic loading test that can comprehensively reflect the bearing capacity and ductility of the components as the engineering demand parameters. This study matched the performance target specified by the Chinese code for non-structural components, and took the yield displacement, the displacement corresponding to the peak force, and the energy value corresponding to the limit displacement as the representative values of the three types of damage levels, respectively, to analyze the fragility of the pipeline system.

(3) Due to the reasonable design of the S1 and M1 specimens, including diagonal bracing and seismic connectors, the S1 and M1 specimens are generally stronger than the S2 and M2 specimens, including the properties of bearing capacity and energy dissipation capacity. For example, the peak bearing capacities of the S1–Y and S2–Y test specimens are 7.27 kN and 2.74 kN, respectively. When the test specimen reaches the DL 1 failure level, the engineering demand parameters (energy value) are 3.45 J and 26.74 J, respectively. It can be seen that the seismic connectors play a vital role in the seismic performance of seismic bracing.

(4) Although the seismic bracings of the S1–X and M1–X test specimens have strong bearing capacity, the connection between the pipes and the pipe clamps is extremely weak. The connections between the pipes and the pipe clamps of the S1–X and M1–X test specimens are damaged when they reach 2.4 kN and 6.3 kN, respectively. It is necessary to focus on improving this problem in order to strengthen the force transmission mode between pipes and pipe clamps or continue to increase their friction. There are still some problems in the practical application of the seismic connectors used for the S2 and M2 test specimens. For example, the connection position of the lower seismic connector and the suspension screw is designed with a gap for convenient installation, but the gap easily causes the seismic connector and the vertical suspension screw to fall off during extremely adverse conditions. In addition, the S2 and M2 seismic connectors easily rotate and loosen at the pre-tensioned bolts, which leads to the yielding of the seismic connectors. These

problems are the result of the overall low bearing capacity of these seismic bracing systems. It is recommended to shorten the manufacturing length of the seismic connectors of this type of test specimen and optimize its force transmission path, thus achieving better seismic effect.

(5) Expansion of the NSC fragility database may make the resilience assessment of important buildings more accurate after earthquakes.

Author Contributions: Methodology, Y.Y.; Formal analysis, W.B.; Writing—original draft, R.L.; Funding acquisition, T.J. and J.D. All authors have read and agreed to the published version of the manuscript.

Funding: The authors disclose receipt of the following financial support for the research, authorship, and/or publication of this article: the Natural Science Foundation of China under Grant No. 52078471, the Natural Science Foundation of China under Grant No. 52208509, the Basic Research Foundation of Institute of Engineering Mechanics, CEA 21 (2019A03), and the Basic Research Foundation of Institute of Engineering Mechanics, CEA (2022C04), the Heilongjiang Provincial Natural Science Foundation (LH2022E121). The materials presented are the research findings by the authors and are not necessarily an expression of the funding agency's opinion.

Conflicts of Interest: The authors declare no conflict of interest.

Appendix A

Hysteresis curve of the S1–Y, S2–X, S2–Y, M1–X, M1–Y, M1–X, and M2–Y specimens.

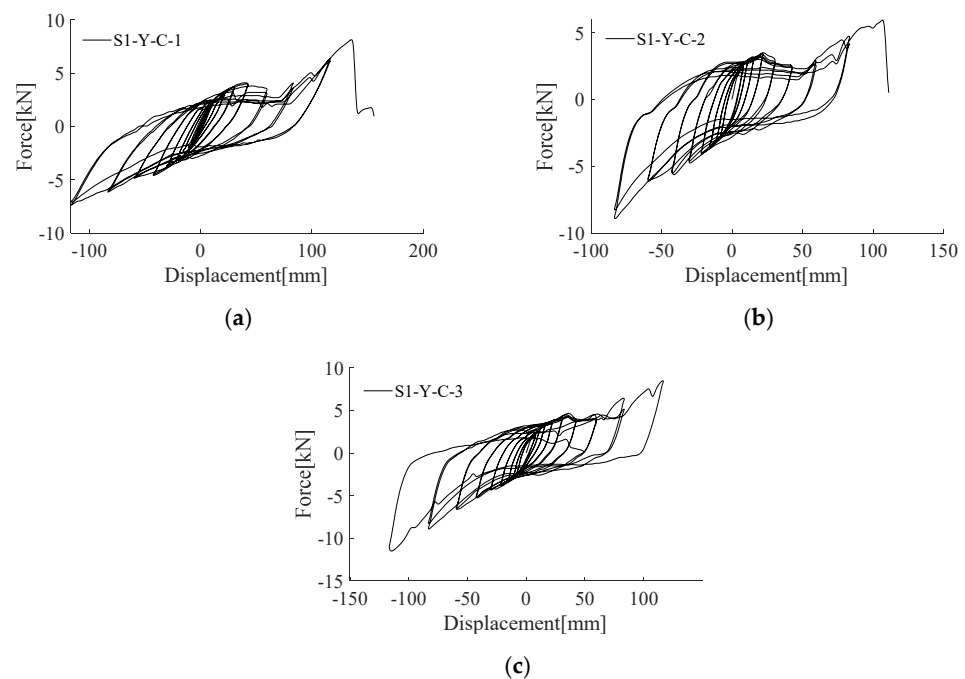


Figure A1. Hysteresis curve of the S1–Y specimens. (a) S1–Y–C–1; (b) S1–Y–C–2; and (c) S1–Y–C–3.

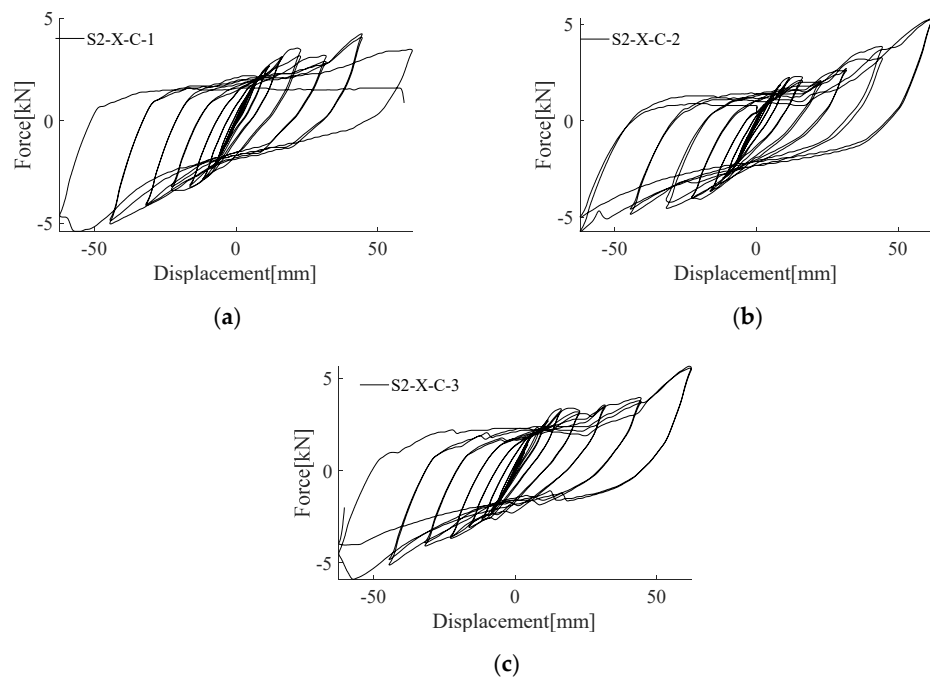


Figure A2. Hysteresis curve of the S2-X specimens without the tube clamp. (a) S2-X-C-1; (b) S2-X-C-2; and (c) S2-X-C-3.

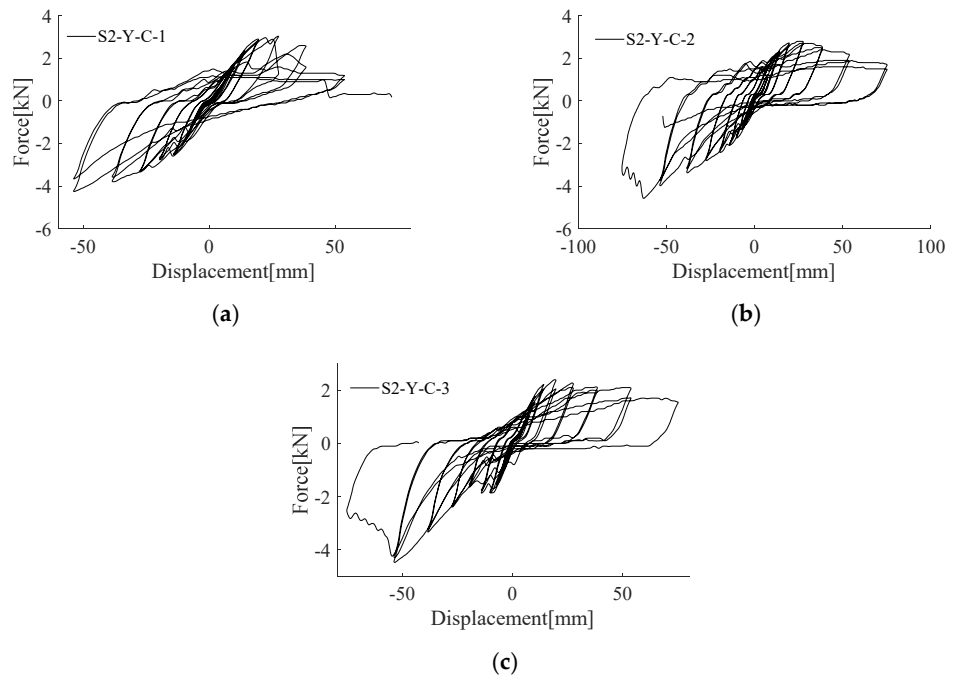


Figure A3. Hysteresis curve of the S2-Y specimens. (a) S2-X-C-1; (b) S2-Y-C-2; and (c) S2-Y-C-3.

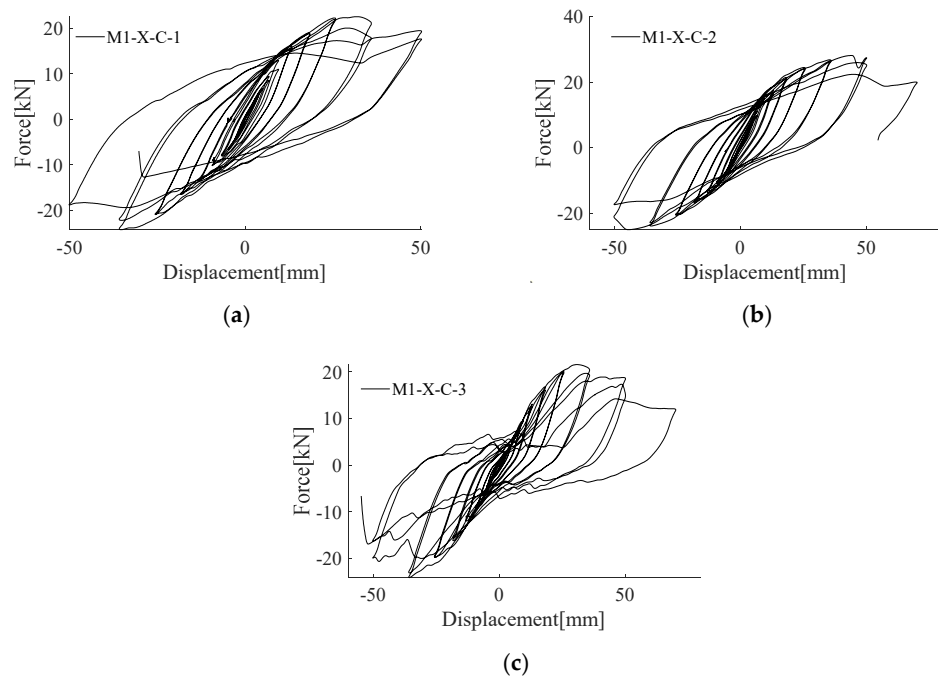


Figure A4. Hysteresis curve of the M1–X specimens without the tube clamp. (a) M1–X–C–1; (b) M1–X–C–2; and (c) M1–X–C–3.

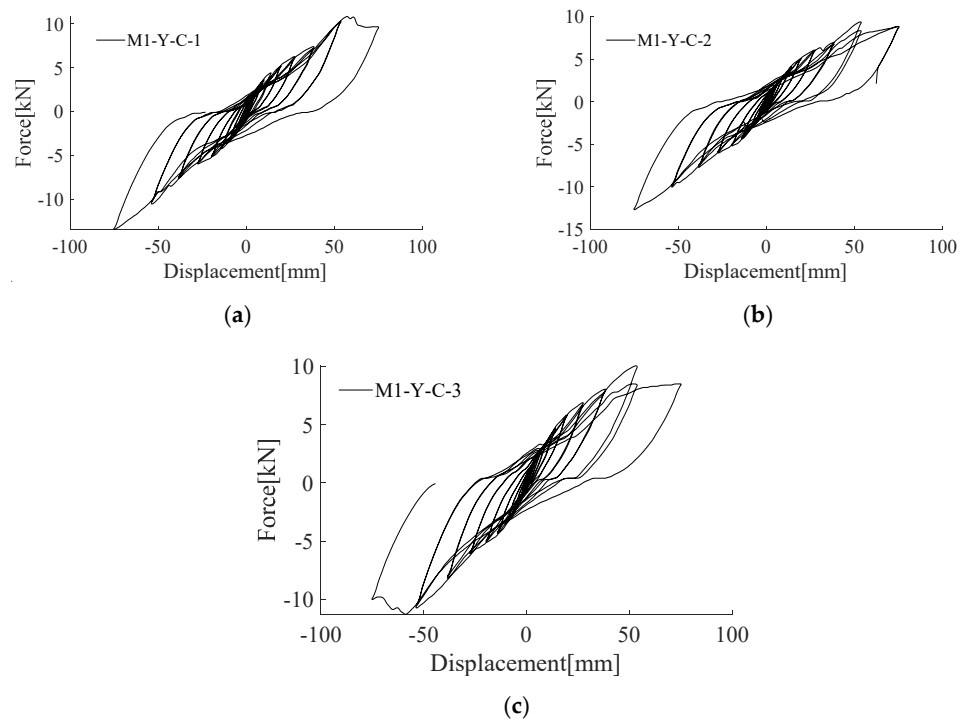


Figure A5. Hysteresis curve of the M1–Y specimens. (a) M1–Y–C–1; (b) M1–Y–C–2; and (c) M1–Y–C–3.

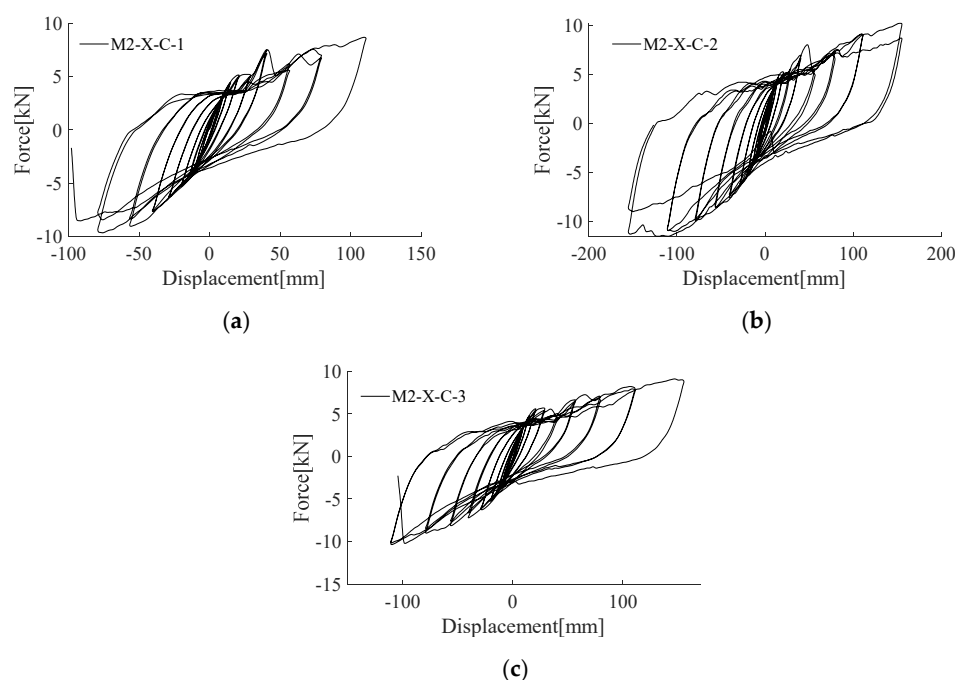


Figure A6. Hysteresis curve of the M2–X specimens without the tube clamp. (a) M2–X–C–1; (b) M2–X–C–2; and (c) M2–X–C–3.

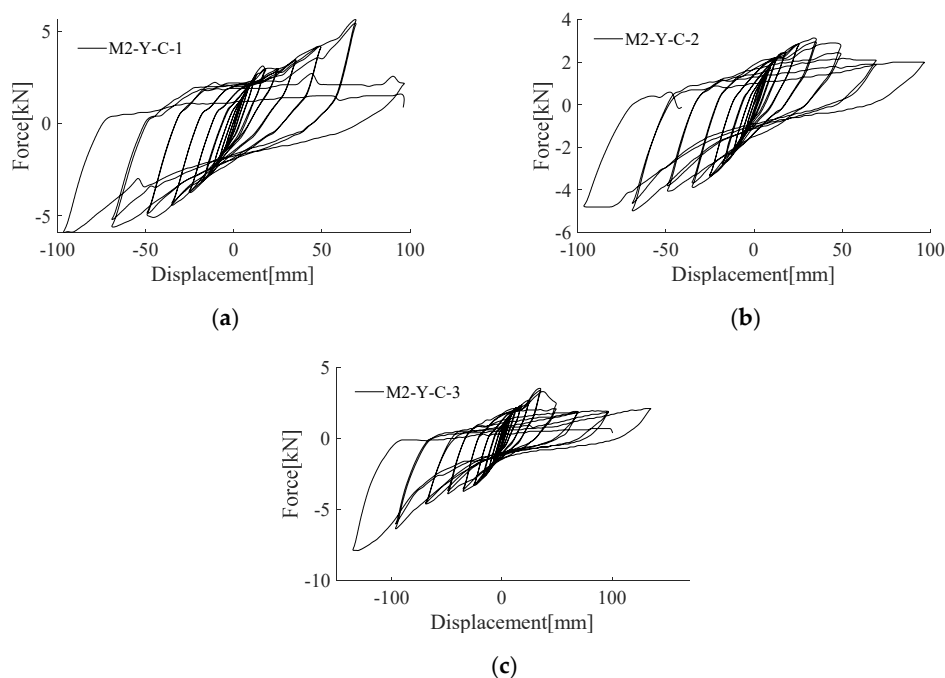


Figure A7. Hysteresis curve of the M2–Y specimens. (a) M2–Y–C–1; (b) M2–Y–C–2; and (c) M2–Y–C–3.

References

1. Morales-Beltran, M.; Engür, P.; Şişman, Ö.A.; Aykar, G.N. Redesigning for Disassembly and Carbon Footprint Reduction: Shifting from Reinforced Concrete to Hybrid Timber–Steel Multi-Story Building. *Sustainability* **2023**, *15*, 7273. [[CrossRef](#)]
2. Sarıtaş, F.; Bedirhanoglu, I.; Konak, A.; Keskin, M.S. Effect of Seismic Isolation on the Performance of High-Rise Buildings with Torsional Instability. *Sustainability* **2022**, *15*, 36. [[CrossRef](#)]
3. D’Amato, M.; Laguardia, R.; Gigliotti, R. Seismic retrofit of an existing RC building with isolation devices applied at base. *Front. Built Environ.* **2020**, *6*, 82. [[CrossRef](#)]

4. Zhou, X.; Zhao, D.; Sun, X.; Yang, X.; Zhang, J.; Ni, T.; Tang, K. An asymmetric quasi-zero stiffness vibration isolator with long stroke and large bearing capacity. *Nonlinear Dyn.* **2022**, *108*, 1903–1930. [[CrossRef](#)]
5. Fema, E. *Reducing the Risks of Nonstructural Earthquake Damage—A Practical Guide*; DIANE Publishing: Darby, PA, USA, 2011; Volume 74.
6. Steinbrugge, K.V.; Schader, E.E. *Earthquake Damage and Related Statistics in San Fernando, California, Earthquake of February 9, 1971*; Murphy, L., Ed.; National Oceanic and Atmospheric Administration: Washington, DC, USA, 1973; Volume 1A, pp. 709–710+713.
7. Baitao, S.; Peilei, Y.; Mingzhen, W. *Atlas of Building Seismic Damage Caused by the Lushan “4 · 20” Ms7.0 Earthquake, Sichuan Province*; Earthquake Press: Beijing, China, 2014. (In Chinese)
8. Chen, S. Preface to the special issue on seismic performance of underground structures: From experiments to analysis. *Earthq. Res. Adv.* **2022**, *2*, 100183. [[CrossRef](#)]
9. Xu, R.; Qu, T.J.; Jiang, R. Longitudinal Seismic Response of Underground Pipelines Subjected to Multiple-Supported Random Ground Excitations. *J. Pipeline Syst. Eng. Pract.* **2022**, *13*, 04021069. [[CrossRef](#)]
10. Ye, J.; Lu, Q. Seismic dynamics of a pipeline shallowly buried in loosely deposited seabed foundation. *Ocean. Eng.* **2022**, *243*, 110194. [[CrossRef](#)]
11. Baolei, Z.; Jianxing, Y.; Zhenzhou, S. Research on Local Pressure Collapse Characteristics of Deep Water Pipeline Under Dynamic Loading. *J. Vib. Shock.* **2017**, *36*, 104–110+133. (In Chinese) [[CrossRef](#)]
12. Tianxiang, L.; Shaokong, F.; Guanlin, Y. Tests for leakage monitoring method of large pressure water pipeline. *J. Vib. Shock.* **2021**, *40*, 136–142. (In Chinese)
13. Tian, Y.; Filiatrault, A.; Mosqueda, G. Seismic response of pressurized fire sprinkler piping systems i: Experimental study. *J. Earthq. Eng.* **2014**, *19*, 649–673. [[CrossRef](#)]
14. Tian, Y.; Filiatrault, A.; Mosqueda, G. Experimental seismic fragility of pressurized fire suppression sprinkler piping joints. *Earthq. Spectra* **2014**, *30*, 1733–1748. [[CrossRef](#)]
15. Hoehler, M.S.; Panagiotou, M.; Restrepo, J.I.; Silva, J.F.; Floriani, L.; Bourgund, U.; Gassner, H. Performance of suspended pipes and their anchorages during shake table testing of a seven-story building. *Earthq. Spectra* **2009**, *25*, 71–91. [[CrossRef](#)]
16. *ASCE 7-05; Minimum Design Loads and Associated Criteria for Buildings and Other Structures*. American Society of Civil Engineers: Reston, VI, USA, 2005.
17. Perrone, D. Experimental seismic response evaluation of suspended piping restraint installations. *Earthq. Spectra* **2020**, *28*, S453–S471. [[CrossRef](#)]
18. *FEMA P-795; Quantification of Building Seismic Performance Factors: Component Equivalency Methodology*. Federal Emergency Management Agency: Washington, DC, USA, 2008.
19. Qingxue, S.; Li, Z.; Liu, R.; Wang, T. Experimental study on properties of aseismic braces used in pipe line systems. *Eng. Mech.* **2018**, *35* (Suppl. S1), 120–125+133. (In Chinese)
20. Wu, H.; Guo, E.; Sun, D.; Mao, C.; Zhang, H.; Liu, Z. Shaking table test of water supply pipes installed in a full-scale masonry structure. *KSCE J. Civ. Eng.* **2022**, *26*, 824–836. [[CrossRef](#)]
21. Sakai, T.; Fujita, K.; Zhang, Y.; Song, Y. Comparative study on seismic design of buildings in Japan and China. *J. Asian Archit. Build. Eng.* **2017**, *16*, 111–118.
22. *FEMA 461; Interim Testing Protocols for Determining the Seismic Performance Characteristics of Structural and Nonstructural Components*. Federal Emergency Management Agency: Washington, DC, USA, 2007.
23. *GB/T 17395-2008; Dimensions, Shapes, Masses, and Tolerances of Seamless Steel Tubes*. Standards Press of China: Beijing, China, 2008. (In Chinese)
24. *FEMA P-58-2; Seismic Performance Assessment of Buildings Volume 2: Implementation Guide*. Federal Emergency Management Agency: Washington, DC, USA, 2012.
25. *JGJ 101-1996; Specificating of Testing Methods for Earthquake Resistant Building*. China Architecture & Building Press: Beijing, China, 1997. (In Chinese)
26. *GB50011-2010; Code for Seismic Design of Buildings*. China Architecture Industry Press: Beijing, China, 2016. (In Chinese)

Disclaimer/Publisher’s Note: The statements, opinions and data contained in all publications are solely those of the individual author(s) and contributor(s) and not of MDPI and/or the editor(s). MDPI and/or the editor(s) disclaim responsibility for any injury to people or property resulting from any ideas, methods, instructions or products referred to in the content.